9548–9567 *Nucleic Acids Research, 2022, Vol. 50, No. 16* *Published online 30 August 2022*
https://doi.org/10.1093/nar/gkac710

Chemically targeting the redox switch in AP1 transcription factor ΔFOSB

Ashwani Kumar[1,2,†], Galina Aglyamova[1,2,†], Yun Young Yim[3], Aaron O. Bailey[4], Haley M. Lynch[5], Reid T. Powell[6], Nghi D. Nguyen[6], Zachary Rosenthal[7], Wen-Ning Zhao[7], Yi Li[1], Jianping Chen[1], Shanghua Fan[1,2], Hubert Lee[1,2], William K. Russell[4], Clifford Stephan[6], Alfred J. Robison[5], Stephen J. Haggarty[7], Eric J. Nestler[3], Jia Zhou[1,2], Mischa Machius[1,2] and Gabby Rudenko[1,2,*]

[1]Department of Pharmacology and Toxicology, University of Texas Medical Branch, Galveston, TX 77555, USA, [2]Sealy Center for Structural Biology and Molecular Biophysics, University of Texas Medical Branch, Galveston, TX 77555, USA, [3]Nash Family Department of Neuroscience and the Friedman Brain Institute, Icahn School of Medicine at Mount Sinai, New York, NY 10029, USA, [4]Department of Biochemistry and Molecular Biology, University of Texas Medical Branch, Galveston, TX 77555, USA, [5]Department of Physiology, Michigan State University, East Lansing, MI 48824, USA, [6]HTS Screening Core, Texas A&M University School of Medicine, Institute of Biosciences and Technology, Center for Translational Cancer Research, Houston, TX 77030, USA and [7]Chemical Neurobiology Laboratory, Center for Genomic Medicine, Massachusetts General Hospital, Departments of Psychiatry & Neurology, Harvard Medical School, Boston, MA 02114, USA.

Received May 24, 2022; Revised July 21, 2022; Editorial Decision July 28, 2022; Accepted August 08, 2022

ABSTRACT

The AP1 transcription factor ΔFOSB, a splice variant of FOSB, accumulates in the brain in response to chronic insults such as exposure to drugs of abuse, depression, Alzheimer's disease and tardive dyskinesias, and mediates subsequent long-term neuroadaptations. ΔFOSB forms heterodimers with other AP1 transcription factors, e.g. JUND, that bind DNA under control of a putative cysteine-based redox switch. Here, we reveal the structural basis of the redox switch by determining a key missing crystal structure in a trio, the ΔFOSB/JUND bZIP domains in the reduced, DNA-free form. Screening a cysteine-focused library containing 3200 thiol-reactive compounds, we identify specific compounds that target the redox switch, validate their activity biochemically and in cell-based assays, and show that they are well tolerated in different cell lines despite their general potential to bind to cysteines covalently. A crystal structure of the ΔFOSB/JUND bZIP domains in complex with a redox-switch-targeting compound reveals a deep compound-binding pocket near the DNA-binding site. We demonstrate that ΔFOSB, and potentially other, related AP1 transcription factors, can be targeted specifically and discriminately by exploiting unique structural features such as the redox switch and the binding partner to modulate biological function despite these proteins previously being thought to be undruggable.

INTRODUCTION

ΔFOSB is a transcription factor responsible for inducing long-term neuroplasticity and behavioral changes. The ΔFOSB protein accumulates in specific brain regions and cell types following many types of chronic stimuli. For instance, ΔFOSB protein levels rise following repeated exposure to reward-inducing stimuli such as drugs of abuse (1–3) and exercise (4) but also in response to chronic insults like repeated stress (5) and seizures associated with Alzheimer's disease (6–8). The high levels of ΔFOSB protein induced by drugs of abuse increase reward-seeking and reward-reinforcing behaviors promoting addiction-like states, whereas they enhance susceptibility or resilience in response to chronic stress depending upon the cell type involved (1,2,9,10). Increased ΔFOSB levels are also linked to aggressive behavior (11), stress-induced binge eating (12) and dyskinesias (abnormal involuntary movements)

*To whom correspondence should be addressed. Tel: +1 409 772 6292; Fax: +1 409 772 9642; Email: garudenk@utmb.edu
†The authors wish it to be known that, in their opinion, the first two authors should be regarded as Joint First Authors.
Present addresses:
Galina Aglyamova, Department of Molecular & Human Genetics, Baylor College of Medicine, Houston, TX 77030, USA.
Wen-Ning Zhao, Vesigen Therapeutics, Cambridge, MA 02139, USA.

that accompany Parkinson's disease (13). ΔFOSB induction can be beneficial and can exhibit protective functions; for example, ΔFOSB induction is required in hippocampus for normal learning (14), elevated ΔFOSB protein enhances resilience in response to chronic stress as noted (1,2,9), while it dampens behavioral sensitization to cocaine following environmental enrichment (15), and it reduces specific forms of nerve pain (16). On the other hand, decreased levels of ΔFOSB can be associated with disease, for instance, in specific brain regions they are linked to depression (10). Overall, ΔFOSB is thought to be a 'molecular switch' that stably alters programs of gene expression for the long term (either as an activator or inhibitor of gene transcription) and thereby induces long-term neuroadaptations and behavioral adaptations in response to chronic (but not acute) stimuli (17,18).

ΔFOSB is an attractive drug target because of its central role in drug addiction, depression, dyskinesias, and seizure-induced cognitive decline as well as its ability to mediate long-term behavioral changes (18). Indeed, genetically or virally reducing ΔFOSB protein levels in the nucleus accumbens diminishes drug addictive behaviors (3), and reducing it more broadly in the striatum decreases tardive dyskinesias seen in Parkinson's disease (19). By contrast, genetically boosting ΔFOSB protein levels in the nucleus accumbens causes long-lasting and significant protection against nerve pain seen in neuropathic allodynia (16). Pharmacological probes targeting ΔFOSB *in vivo* would be of great value for interrogating the exact molecular mechanisms of ΔFOSB action in general and in different disease pathologies. Such probes, upregulating or downregulating ΔFOSB function, would avoid many of the confounds that genetic or viral manipulations can bring, e.g. their region-specific nature and the compensatory effects that are induced upon overexpression or knockdown strategies. Chemical probes targeting ΔFOSB could also be leveraged to assess the utility of ΔFOSB as a therapeutic target.

ΔFOSB is a member of the activator protein 1 (AP1)-family of transcription factors. It is an alternative splice variant of the FOSB gene and lacks the C-terminal 101 residues found in full-length FOSB (3). ΔFOSB works both as an activator as well as an inhibitor of gene expression, but the molecular bases of these opposing actions are not well understood (1). The ΔFOSB protein accumulates in the brain with a half-life of ∼7 days, compared to FOSB and all other FOS family proteins, which have a half-life of several hours at most (9,20). The unique stability of ΔFOSB is largely the result of the absence of two degron domains found in FOSB (21) and phosphorylation of specific serine residues, in particular Ser27 (20,22). ΔFOSB, like all AP1 transcription factors, contains a basic leucine zipper (bZIP) domain consisting of an N-terminal basic region and a C-terminal leucine zipper. Dimerization with another bZIP transcription factor leads to the formation of a DNA-binding site (23–25). For instance, in medium spiny neurons, which represent ∼95% of the neurons in the striatum, the main partner of ΔFOSB is thought to be JUND, although the latter does not accumulate in response to chronic stimuli (6,26). *In vitro*, ΔFOSB can also form homomers (such as dimers and tetramers), although their significance *in vivo* is not yet known (25). The DNA-binding regions in the

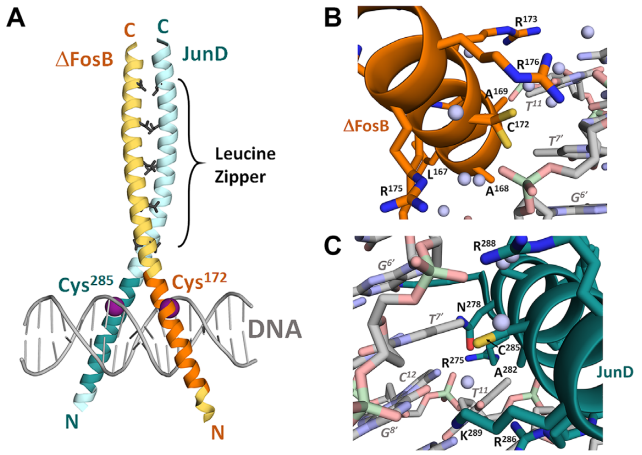

Figure 1. Three-dimensional structure of the ΔFOSB/JUND bZIP region. (**A**) ΔFOSB/JUND/DNA complex (PDB ID 5VPE). ΔFOSB is shown in orange, JUND in cyan. N- and C-termini are indicated. DNA-binding motifs are shown in more intense colors, DNA in grey. ΔFOSB Cys^{172} and JUND Cys^{285}, which form a putative redox switch, are indicated as magenta spheres. Leucine-zipper leucine residues are shown in dark grey. (**B**) Close-up of the ΔFOSB DNA-binding region spanning Arg^{161}-Arg^{177} that contains ΔFOSB Cys^{172} and the DNA-binding motif Asn^{165}-Arg^{173}. The Cys^{172} side chain was modeled in two conformations in the crystal structure to reflect the electron density that clearly showed the two alternative conformations. (**C**) Close-up of the JUND DNA-binding region spanning Arg^{275}-Lys^{289} that contains JUND Cys^{285} and the DNA-binding motif Asn^{278}-Arg^{286}. In (B) and (C), the DNA base numbering is italicized; water molecules are shown as light blue spheres; atom color scheme: carbon, orange (ΔFOSB), cyan (JUND), grey (DNA); oxygen, red (protein), pink (DNA); nitrogen, blue (protein), light blue (DNA); phosphate, green and cysteine, yellow.

ΔFOSB/JUND heterodimer insert into the major groove of DNA (Figure 1A) specifically recognizing the AP1 DNA consensus sequence (AP1 site) in select gene promoters and enhancers (Figure 1B and C) (24). Strikingly, single cysteine residues are found in the DNA-binding portion of both bZIP domains (ΔFOSB Cys^{172} and JUND Cys^{285}). In the DNA-bound state, these residues are about 14 Å apart and are very close to DNA but they do not interact directly with it (Figure 1) (24). While no high-resolution structural information is available for the DNA-free, active state of ΔFOSB/JUND, it is known that, in absence of DNA, these cysteines are prone to oxidation; the structure of ΔFOSB/JUND in the oxidized, DNA-free form reveals a disulfide bond that kinks the central ΔFOSB α-helix (24). This kink deforms and closes the DNA-binding site so that it can no longer insert into the DNA major groove. This structural transition is likely the basis of a redox switch that was proposed in the related AP1 transcription factor c-FOS/c-JUN and that was suggested to regulate DNA binding in cell-based studies (24,27).

Transcription factors are typically flexible proteins that lack well-formed, deep, functional pockets (like catalytic sites in enzymes) and thus are generally considered 'undruggable' or difficult to target with small molecules. In recent years, the covalent modification of critical residues, such as cysteines, with small molecules has emerged as a key strategy to target some undruggable proteins, and tens of FDA-approved drugs are known to work as covalent mod-

ifiers achieving sufficient specificity to be useful medications (28,29). Due to its strategic location, the redox switch of ΔFOSB would constitute an attractive molecular target to regulate its DNA-binding properties and function or to broadly inactivate accumulated pathogenic forms of ΔFOSB. It is currently not known whether the redox switch of ΔFOSB can be exploited in this manner. The DNA-binding regions where the redox-switch cysteines are located are thought to be disordered in absence of DNA. Furthermore, it is not known whether the protein environment surrounding these cysteines allows for the specific and selective binding of covalent modulators. Here we: (i) reveal the first three-dimensional structure of the ΔFOSB/JUND bZIP heterodimer in the DNA-free, active form; (ii) use high-throughput screening (HTS) to identify compounds that target the redox-switch cysteines in ΔFOSB/JUND heterodimers and ΔFOSB homomers; (iii) identify two classes of cysteine-reactive hits and validate them using a panel of assays; (iv) reveal the three-dimensional structure of the ΔFOSB/JUND bZIP heterodimer in complex with a redox-switch-seeking compound; (v) demonstrate that our compounds are well tolerated in cell-based assays and impact the expression of an AP1-reporter gene and (vi) demonstrate that the redox-switch cysteines are located in a pocket that may support the rational design of selective small molecules that modulate the ability of ΔFOSB to regulate the expression of target genes.

MATERIALS AND METHODS

Reagents

- *Cysteine-focused thiol-reactive compounds*. A 'cysteine-focused covalent fragments library' (Enamine; Monmouth Jct., NJ) with 3200 compounds was plated in 384-well plates at 10 mM in DMSO. Additional compounds were purchased from commercial vendors: Z2159931480, Z291278830, Z3247353427, Z2492395544 and 1183031-77-7 (Enamine; Monmouth Jct., NJ), 2196-99-8 (Sigma Aldrich; St. Louis, MO) and 456-04-2 (TCI America, Inc., Portland, OR).
- *Oligonucleotides*. The 19-mer *cdk5* oligonucleotide ('*cdk5* oligo') contains the forward and reverse strands of 5′-CGTCGGTGACTCAAAACAC-3′ (AP1 site underscored) derived from the AP1 site in the cyclin-dependent kinase 5 promoter. The TMR-*cdk5* oligo was generated by annealing equivalent molar quantities of the complementary strands each labeled with TAMRA (Sigma Aldrich) at the 5′-end and heating them to 95°C for 2.5 min, followed by slow cooling to room temperature (roughly 1 min/°C) and storage at −20°C as 50 μM stocks in annealing buffer (10 mM Tris pH 8, 50 mM NaCl). For electrophoretic mobility shift assays (EMSAs), the biotinylated forward strand of the *cdk5* oligo and the unlabeled reverse strand *cdk5* oligo (Sigma) were annealed as above yielding oligonucleotide 'BIO-*cdk5*'.
- *Antibodies*. Rabbit anti-FOSB antibody: Cell Signaling Technology; Danvers, MA; catalog # 2251. Mouse anti-β-actin antibodies: Cell Signaling Technology; Danvers, MA; catalog # 3700. Horseradish peroxidase (HRP)-conjugated secondary goat anti-mouse antibodies: SeraCare; Milford, MA; catalog # 5220-0341. Horseradish peroxidase (HRP)-conjugated secondary goat anti-rabbit antibodies: SeraCare; Milford, MA; catalog # 5220–0337.

Biological resources

- AP1 luciferase reporter human embryonic kidney 293 recombinant cell line (AP1-luc HEK293): BPS Bioscience; San Diego, CA; catalog # 60405.
- Human microglial clone 3 (HMC3) cell line: ATCC; Manassas, VA; catalog # CRL-3304.
- Human fibroblasts: Coriell Institute for Medical Research, Camden, NJ; catalog # GM08330.

Protein expression and purification

For compound screening and validation including dose-response curves (DRCs) and EMSAs, full-length ΔFOSB/JUND and ΔFOSB were used. Full-length ΔFOSB $Cys^{172}Ser$/JUND heteromers and ΔFOSB $Cys^{172}Ser$ homomers were also used for compound testing in fluorescence polarization (FP)-DRCs and ΔFOSB $Cys^{172}Trp$ homomers were used in FP-based studies of binding to the *cdk5* oligo. N-terminally His-tagged mouse ΔFOSB, $N(His)_6$-ΔFOSB, a splice form of FOSB (UniProt ID P13346; tag = MGHHHHHHAG followed by residues Phe^2–Glu^{237}) and N-terminally His-tagged mouse JUND, $N(His)_6$-JUND (UniProt ID J04509; tag = MGHHHHHH followed by residues Glu^2-Tyr^{341}), or mutants, were expressed in Sf9 cells (Bac-to-Bac system, Invitrogen) and purified as previously described (23,30). ΔFOSB/JUND complexes were generated either by mixing the Ni-immobilized metal affinity chromatography (IMAC, Invitrogen) eluate of each protein in a 1:1 ratio, followed by ion-exchange and size-exclusion chromatography, or by co-infecting Sf9 cells with $N(His)_6$-ΔFOSB (MOI ∼1–1.5) and $N(His)_6$-JUND baculoviruses (1:1 or 1:3 with respect to $N(His)_6$-ΔFOSB) followed by purification of the complex. Briefly, flash-frozen cell pellets from 6 L insect culture were thawed, lyzed by sonication (in 20 mM Tris pH 8, 0.2% (v/v) Triton X-100, 1 mM TCEP, 0.5 mM PMSF, 10 μg/ml leupeptin, 10 μg/ml pepstatin A), and an end concentration of 300 mM NaCl, 5 mM $MgCl_2$ and 50 μg/ml DNAse added. Subsequently, the sodium chloride concentration was increased to 1 M, and 0.5 M NaBr and 5 mM imidazole were added before high-speed centrifugation and subsequent Ni-IMAC. Ni-IMAC-purified proteins were diluted to 0.1–0.2 mg/ml, dialyzed overnight in 25 mM Tris pH 9.0, 300 mM NaCl, 1 mM TCEP (or 5 mM DTT), 0.5 mM PMSF, 0.5% (v/v) glycerol, and then dialyzed for 3 h in a low-salt buffer (25 mM Tris, 40 mM NaCl, 1 mM TCEP, 0.5 mM PMSF, 0.5% glycerol, pH 9.0) before purification with anion-exchange chromatography (Mono-Q; GE Healthcare). As a final step, proteins were purified by size exclusion chromatography on a HiLoad 16/600 Superdex 75 pg column (GE Healthcare) equilibrated with 20 mM Tris pH 8.0, 1 M NaCl, 1 mM TCEP. For ΔFOSB:JUND, fractions were checked by SDS-PAGE during protein purification to make sure both proteins were present in a 1:1 complex. Protein purity was also assessed by SDS-PAGE on 12% gels. ΔFOSB/JUND

and ΔFOSB were stored in 20 mM Tris pH 8.0, 1 M NaCl, 1 mM TCEP, typically at 3–5 mg/ml as flash-frozen aliquots.

For mass spectrometry and structural studies, the ΔFOSB bZIP (mouse/human; residues Glu^{153}-Lys^{219} containing Cys^{172}) and JUND bZIP (mouse; residues Gln^{260}-Val^{326} containing Cys^{279}, which are identical to human Gln^{266}-Val^{332} containing Cys^{285}) were used. The amino-acid sequences of the bZIP domains for ΔFOSB and JUND are fully conserved between mouse and human, and the human residue numbering convention was used here. The proteins were expressed as previously described (24,25). Briefly, the constructs were sub-cloned into a pET21-NESG expression vector with N-terminal hexa-His $(His)_6$-tag followed by a tobacco etch virus (TEV) protease cleavage site and expressed in *Escherichia coli* Rosetta 2 (DE3) cells (Invitrogen). To express recombinant proteins, transformed cells were grown in LB medium at 37°C to O.D. ∼0.6, induced overnight with 0.5–1 mM isopropyl β-D-thiogalactoside at 16°C. The cells were harvested, resuspended, lyzed by sonication, and treated with DNAse (50 μg/ml) in 20 mM Tris pH 8.0, 1 M NaCl, 0.5 M NaBr, 1 mM Tris(2-carboxyethyl)-phosphine (TCEP), 5 mM $MgCl_2$, 20 mM imidazole; the lysate was then centrifuged at 18 000 rpm for 30 min. The proteins were purified by Ni-IMAC using a Ni-NTA agarose column (Invitrogen) and the $(His)_6$-tag removed by incubating the protein with His-tagged TEV protease for 3 h at room temperature in 50 mM Tris pH 8, 500 mM NaCl, 1% glycerol and 1 mM DTT. To remove the cleaved His-tag, uncleaved protein, and His-tagged TEV, the sodium chloride concentration was increased to 1 M, the protein subjected again to Ni-IMAC, and the flow-through containing the His-tag-free protein collected. The bZIP domains of ΔFOSB and JUND were then combined in a 1:1 molar ratio, dialyzed against 20 mM HEPES pH 7.0, 0.5 M NaCl overnight at room temperature and then subjected to size-exclusion chromatography on a HiLoad 16/600 Superdex 75 pg column (GE Healthcare) equilibrated with 20 mM HEPES, 0.5 M NaCl, pH 7.0. Fractions were checked by SDS-PAGE to ensure both proteins were present, and protein purity was assessed by SDS-PAGE on 12% gels. Protein concentrations were generally determined by a Bradford assay (BioRad Protein Assay), not via UV absorption based on extinction coefficients due to the absence of tryptophan and tyrosine residues. ΔFOSB/JUND was concentrated to 5–10 mg/ml and stored in 20 mM Tris pH 8, 1 M NaCl as flash-frozen aliquots.

High-throughput compound screening

We screened the cysteine-focused covalent fragments library (3200 compounds) using a fluorescence polarization (FP) assay adapted for high-throughput screening that monitors the binding of full-length N$(His)_6$-ΔFOSB/N$(His)_6$-JUND heteromers ('ΔFOSB/JUND') and, in parallel, N$(His)_6$-ΔFOSB homomers ('ΔFOSB'), to TMR-*cdk5*, as previously described (23,30). For the primary screen, one dose of compound was transferred from library stock plates to 384-well assay plates (Corning, #3676) using an Acoustic Liquid Transfer Machine Echo 550 (Beckman) for a final concentration of 50 μM. Subsequently, TMR-*cdk5* oligo was added to all wells (25 nM final concentration). Then, in parallel, ΔFOSB/JUND (280 nM monomer concentration), ΔFOSB (320 nM monomer concentration), or a 'no protein' control (buffer only) was added to the wells with compounds/oligonucleotides (in 20 mM HEPES pH 7.5, 150 mM NaCl for ΔFOSB/JUND and 20 mM HEPES pH 7.5, 50 mM NaCl for ΔFOSB, respectively) for a total volume of 20 μl, and the plates incubated for 15 min at room temperature. DMSO was backfilled into control wells to maintain a constant concentration of 2% (v/v). Fluorescence was measured using a BioTek, Synergy Neo2 plate reader (excitation 530 nm, emission 590 nm). In each plate, wells with TMR-*cdk5* alone were used as 'positive' controls (representing 100% inhibition and 0% protein:DNA binding), while wells with TMR-*cdk5* incubated with 280 nM ΔFOSB/JUND or 320 nM ΔFOSB but no compound, were used as negative controls (representing 0% inhibition and 100% protein:DNA binding). Compound C1 (Chembridge 6572652) was used as a reference active compound to calculate quality-control and assay-performance metrics (30).

Assay-quality-control metrics were calculated throughout the screening campaign according to procedures in the Assay Guidance Manual (31). For screening compounds against ΔFOSB/JUND heteromers, the FP signal window was 64.50 ± 3.75 mP with very low technical noise (mean coefficient of variance 1.2 ± 0.11% for the negative controls and 1.80 ± 0.27% for the positive controls) and a robust *Z*' score of 0.76 ± 0.05. Similarly, for screening compounds against ΔFOSB homomers, the FP signal window was 65.50 ± 1.50 mP with a mean coefficient of variance of 1.36 ± 0.17% and 2.0 ± 0.21% for the negative and positive controls, respectively, and a *Z*' score of 0.74 ± 0.03.

Hit calling was performed using a rule-based classifier. The first-pass criterion removed non-specific binding of the compounds to the TMR-*cdk5* oligo by setting a maximal activity filter on the fluorescence-polarization reading before the addition of the protein, which was objectively set to retain only compounds for which, in presence of DNA, the absolute value for fluorescence polarization (anisotropy) |FA| was ≤0.1 (i.e. ≤10% difference from the positive control, TMR-*cdk5*, alone).

$$\mathrm{FA} = 1 - \left(\frac{\mathrm{FP}_{ij}}{\langle \mathrm{FP} \rangle_{\mathrm{cdk5+DMSO}}} \right),$$

whereby FP_{ij} is the fluorescence polarization value for each assay well position and $<FP>_{cdk5+DMSO}$ is the median fluorescence polarization of the wells containing buffer including 2% DMSO and the TMR-*cdk5* oligo.

The second-pass filter prioritized hits by selecting compounds with a high ability to disrupt the binding of protein to DNA, which was defined here as a Score of ≥0.75. This value was calculated by first normalizing the FP signal from each assay well by subtracting the median value of the on-plate negative control (*cdk5* oligo +protein in buffer + DMSO, i.e. no compound effect, full protein:DNA binding) and then scaling it to the difference between the median FP signal of the on-plate positive (*cdk5* oligo alone, i.e. fully unbound) and negative controls (*cdk5* oligo + protein), us-

ing the following formula.

$$\text{Score} = \frac{FP_{ij} - \langle FP\rangle_{\text{protein+cdk5}}}{\langle FP\rangle_{\text{cdk5+DMSO}} - \langle FP\rangle_{\text{protein+cdk5}}},$$

whereby FP_{ij} is the normalized and scaled fluorescence polarization for each assay well position; $<FP>_{\text{cdk5+DMSO}}$ is the median fluorescence polarization of the wells containing the TMR-*cdk5* oligo; and $<FP>_{\text{protein+cdk5}}$ is the median fluorescence polarization of wells containing ΔFOSB/JUND or ΔFOSB and TMR-*cdk5* oligo. Medians are used here over the mean value to make the analysis more robust to outliers that may be present in empirically collected data.

Fluorescence polarization dose-response curves

Candidate compounds identified in our initial screen were purchased from vendors (see above) and tested in a 10-point dose-response assay to validate the hit status and obtain an estimate of their IC_{50} values, as we have done before (30,32). A serial dilution of compound (0–200 μM) was dispensed into 384-well microtiter plates (Corning, #3676) using an Acoustic Liquid Transfer Machine Echo 550 (Beckman) or manually. Subsequently, 25 nM TMR-*cdk5* oligo was added to each well. DRC assays were carried out in quadruplicates for ΔFOSB/JUND (FP-buffer: 280 nM in 20 mM HEPES pH 7.5, 150 mM NaCl), in quadruplicates for ΔFOSB (FP-buffer: 320 nM in 20 mM HEPES, pH 7.5, 50 mM NaCl,) or in duplicates without protein. Samples were incubated for 15 minutes at room temperature and the FP signal measured using a Synergy Neo2 plate reader (BioTek, excitation 530 nm, emission 590 nm) or Pherastar plate reader (BMG LabTech, excitation 540 nm, emission 590 nm). Each 384-well plate also included 8 positive control wells (TMR-*cdk5* alone) and 8 negative control wells (ΔFOSB + TMR-*cdk5*) in the appropriate FP buffer (including 2% DMSO, which we ascertained did not impact the assay). The concentration series of compound with TMR-*cdk5* but no protein served to identify compounds interfering with the assay or binding to TMR-*cdk5* directly. Data were processed with Prism6 (GraphPad) using the 'log(inhibition) versus response-variable slope (four parameters)' algorithm model to estimate the IC_{50}.

Electrophoretic mobility gel shift assay (EMSA)

The ability of compounds to disrupt DNA binding was assessed with EMSAs using the Thermo Scientific LightShift EMSA Optimization and Control Kit. Full-length ΔFOSB/JUND (50 or 100 nM) and 5 nM biotinylated oligonucleotide (BIO-*cdk5*) were incubated with 0, 1, 10, 20 or 50 μM compound in 10 mM Tris pH 8.0, 100 mM NaCl, 30 mM KCl, 1 mM EDTA, 10 μg/ml BSA, 2.5% glycerol, 0.1% NP40. The samples 5 nM BIO-*cdk5* oligo (0% shifted) and ΔFOSB/JUND + BIO-*cdk5* (100% shifted), both with no compound added, served as controls. The samples were incubated for 15 min at room temperature, supplemented with bromophenol loading dye (3% Ficoll, 0.02% bromophenol, 0.25× TBE buffer), and then electrophoresed on pre-run 5% native gels on ice at 100 V in 0.5× TBE buffer (44.5 mM Tris, 44.5 mM boric acid, and 1 mM EDTA, pH 8.3). Gels were electroblotted onto positively charged nylon membranes (Invitrogen) in 0.5× TBE at 50 V for 40 min at 4°C and the blots were UV-treated for 10–12 min to cross-link the protein/DNA complexes to the membrane. Chemiluminescence detection of the BIO-*cdk5* oligo was performed according to the manufacturer's instructions (Thermo Scientific™ Pierce™ Chemiluminescent Nucleic Acid Detection Module), using streptavidin–horseradish peroxidase conjugate (1:300 dilution) together with a luminol/enhancer solution and a peroxide solution. Membranes were exposed briefly to X-ray film (Kodak BioMax Light) and the film developed.

Mass spectrometry

Samples for mass spectrometry analysis were prepared as follows. ΔFOSB/JUND bZIP diluted to 2 mg/ml with 20 mM HEPES pH 7, 250 mM NaCl, was treated with 1 mM TCEP and then incubated with 500 μM compound (20 mM stock in DMSO) for 1 h on ice. The samples were then dialyzed for 30 min at 4°C against 20 mM HEPES pH 7, 250 mM NaCl (no TCEP) in a microlyzer with 3.5 kDa molecular weight cut-off (Amicon). Compound was added a second time (500 μM end concentration) and the sample incubated again for 10 minutes on ice. Samples were then centrifuged at 13 000 rpm, the supernatant separated, and its protein concentration measured with the Biorad Protein Assay. Protein-compound complexes were aliquoted, and flash frozen for storage.

Intact mass LC–MS analysis was carried out as follows. Samples containing ΔFOSB/JUND bZIP:compound complexes were analyzed by nanoflow liquid chromatography–tandem mass spectrometry (nano LC-MS/MS) with an UltiMate 3000 RSLC coupled to an Orbitrap Fusion mass spectrometer (Thermo Fisher Scientific) using a Nano-flex ion source. Detailed experimental methods and data analysis are described in the Supplemental Material.

Identification of the Z2159931480 binding site in the ΔFOSB/JUND bZIP domains was achieved by peptide mapping the ΔFOSB/JUND bZIP:Z2159931480 complex via LC–MS/MS analysis. A sample containing ΔFOSB/JUND bZIP:Z2159931480 prepared as described above was denatured in a solution of 5% SDS in 50 mM tetraethylammonium bromide (TEAB), reduced with10 mM TCEP, and alkylated with 20 mM iodoacetamide (IAA). The reduced/alkylated sample was diluted in a 9:1 methanol:50 mM TEAB solution and then loaded onto an S-Trap device where proteins were trypsin-digested using an enzyme-to-substrate ratio of 1:20 for 2 h at 47°C. Digested peptides were recovered from the S-trap using a sequence of elution steps as follows: (i) 50 mM TEAB, (ii) 0.1% formic acid (FA) in H_2O, (iii) 0.1% in 50% in acetonitrile (ACN) and (iv) 0.1% FA in 80% ACN. The combined peptide solution was then dried using a SpeedVac vacuum concentrator and resuspended in 2% acetonitrile, 0.1% formic acid, 97.9% water and placed in an autosampler vial and analyzed by nanoLC–MS/MS using a Thermo Orbitrap Eclipse mass spectrometer equipped with a FAIMS Pro differential ion mobility interface (Thermo Fisher Scientific). Detailed experimental methods are described in the Supplemental Material.

For data analysis, tandem mass spectra were extracted and charge-state deconvoluted using BioPharma Finder (version 4.1.53.14, Thermo Fisher Scientific). All MS/MS spectra were searched against protein sequence databases of the ΔFOSB and JUND bZIPs (taking possible modifications into account like oxidation (Cys, Met), carbamidomethyl (Cys), deamidation (Asn, Gln), and loss of HCl to Z2159931480) using the MassAnalyzer algorithm embedded in BioPharma Finder (33,34). Searches were performed with an MS Noise Level of 2000 and an S/N threshold of 10, parent ion tolerance of 10 ppm, and an MS/MS Minimum Confidence Level of 95%. Trypsin was selected as the protease with a 'High' specificity setting.

Crystallization and X-ray data collection

ΔFOSB/JUND bZIP crystals were grown at 293 K with the hanging-drop vapor-diffusion method by mixing 2–4 μl of ΔFOSB/JUND bZIP (8–10 mg/ml in 20 mM HEPES pH 7.0, 250 mM NaCl with 1 mM TCEP, in presence or absence of thiol-reactive compounds of interest at a stoichiometric ratio of 1:1 to 1:5) with an equal volume of reservoir solution consisting of either 100 mM Tris pH 8.5, 35% (v/v) isopropanol or 100 mM Tris pH 7.0, 40% (v/v) ethanol. Crystals grew within 7 days to a final size of 0.1–0.3 mm. They were cryo-protected in reservoir solution supplemented with 15–20% (v/v) glycerol and then flash-cooled by plunging into liquid nitrogen. Diffraction data sets were collected from single crystals at beamline 5.3 at the Advanced Light Source (Lawrence Berkeley National Laboratory, Berkeley, CA) and at the IMCA beamline at the Advanced Photon Source (Argonne National Laboratory, Argonne, IL), respectively. Crystals exhibited the symmetry of space group I_{222} with cell parameters of a ∼48 Å, b ∼67–69 Å, c ∼122–123 Å, contained one heterodimer in the asymmetric unit, and diffracted X-rays to a d_{min} of about 1.8 Å. However, the diffraction from these crystals was characterized by pronounced anisotropy with severity and impact on overall data completeness varying from crystal to crystal. In addition, diffraction was impacted by fiber-like diffraction patterns that shadowed some of the reflections, as we have observed before (25).

Structure determination, experimental phasing and structural analysis

Data were processed with HKL2000 (35) or with XDS (36,37). Anisotropy correction was carried out with STARANISO (http://staraniso.globalphasing.org/cgi-bin/staraniso.cgi). For ΔFOSB/JUND^{red}, two data sets were used. We determined the initial structure using a data set to 2.4 Å obtained from a crystal grown in presence of TCEP and absence of compounds; at the latter stages, a much higher resolution data set was collected to 1.94 Å from crystals grown in presence of TCEP and an unrelated compound that doesn't bind ΔFOSB/JUND. The '2.4 Å' and '1.9 Å' structures were nearly identical, but the latter gave a more stable refinement of the model and was of higher resolution. For ΔFOSB/JUND^{cmpd}, a single crystal containing compound Z2159931480 was used for structure determination and model refinement. For ΔFOSB/JUND^{red}, data without anisotropic correction were used. Data for ΔFOSB/JUND^{cmpd} were subjected to anisotropic correction, giving diffraction limits along the principal axes of the ellipsoid fitted to the diffraction cut-off surface using a local mean $I/\sigma(I)$ of 1.2 of 3.24 Å (a^*), 4.39 Å (b^*) and 2.26 Å (c^*), respectively. Resolution cutoffs for the final data sets used in structure determination and refinement were applied to ascertain satisfactory completeness overall and in the highest-resolution shell (Table 1).

Table 1. X-ray data collection and structure determination statistics

Crystal	ΔFOSB/JUND^{red}	ΔFOSB/JUND^{cmpd}
Data collection		
Wavelength (Å)	1.000 Å	1.000 Å
Space group	I_{222}	I_{222}
Cell dimensions		
a, b, c (Å)	47.94, 70.24, 122.20	48.26, 67.67, 122.94
α, β, γ (°)	90, 90, 90	90, 90, 90
Anisotropic correction	N/A	Staraniso
Resolution (Å)	33.23–1.94 (1.97–1.94)	44.92–2.45 (2.78–2.45)
Mean $I/\sigma(I)$	32.9 (3.6)	6.7 (1.3)
Completeness spherical (%)	84.1 (25.1)	39.4 (7.9)
Completeness ellipsoidal (%)	N/A	84.9 (72.7)
Multiplicity	11.0 (5.6)	7.2 (7.0)
R_{merge}	0.057 (0.263)	0.216 (2.61)
R_{meas}	0.070 (0.352)	0.233 (2.804)
R_{pim}	0.020 (0.120)	0.085 (1.019)
$CC_{1/2}$	0.989 (0.959)	0.996 (0.664)
Total reflections	146,514 (1083)	22,180 (1344)
Unique reflections	13,357 (194)	3,060 (191)
Refinement		
Resolution (Å)	33.23–1.94 (2.14–1.94)	33.83–3.21 (3.33–3.21)
R_{work}/R_{free}	0.2045/0.2673 (0.2024/0.2788)	0.2791/0.3329 (0.3678/0.5198)
Reflections used R_{work}/R_{free}	11 335/565 (364/18)	2507/191 (116/9)
Completeness (%)	72.48 (23.38)	71.28 (34.42)
Amino acid residues	132	132
Non-hydrogen atoms	1269	1041
Protein/macromolecules	1108	1022
Solvent	154	0
Ligand	13	28
B factors (Å^2), overall	28.53	40.65
Protein/macromolecules	28.16	40.49
Solvent	30.61	-
Ligand	42.13	48.91
TLS groups	2	2
r.m.s. deviations		
bond lengths (Å)	0.011	0.009
bond angles (°)	1.05	1.09
Ramachandran plot (%)		
Favored	100.0	95.3
Allowed	0.0	4.7
Disallowed	0.0	0.0
Rotamer outliers, n (%)	0.0	0.97
Clashscore	3.07	8.71

The crystal structure of ΔFOSB/JUND^{red} was determined by molecular replacement with a poly-alanine model based on the structure of ΔFOSB/JUND bZIP in presence of DNA (PDB ID: 5VPF) as the search model using Phaser as implemented in the Phenix program package (38,39). The resulting model was then used to determine the structure of ΔFOSB/JUND^{red}. Refinements were carried out in Phenix, interspersed with manual rebuilding using COOT (40), and included Translation-Libration-Screw rotation (TLS) parameterization. The models were validated with MolProbity (41). Ramachandran plot statistics (favored/allowed/disallowed) of the final models are: ΔFOSB/JUND^{red} (100.0%/0.0%/0.0%), and ΔFOSB/JUND^{cmpd} (95.3%/4.7%/0.0%). The refined structures exhibit relatively high R_{work} and R_{free} values, most likely due to the above-mentioned diffraction patholo-

gies. For detailed statistics for data collection and refinement see Table 1.

Cell-based reporter assays

The AP1 luciferase reporter human embryonic kidney 293 recombinant cell line (AP1-luc HEK293) was obtained from BPS Bioscience (USA), cultured with growth medium 1B (BPS Bioscience) containing 10% fetal bovine serum (Invitrogen) and 1% penicillin/streptomycin (Hyclone), and incubated at 37°C in 5% CO_2. AP1 reporter luciferase assays were used to determine the effects of compounds on the transcriptional activity of a stably integrated AP1-response-element-driven luciferase reporter gene. The cells were plated in quadruplicates in two 48-well microplates at a concentration of 6.0×10^4 cells/well and incubated for 24 hrs. After stabilizing the cells, the medium was changed to assay medium 1B (BPS) containing 0.5% FBS to starve the cells for 24 h. Subsequently, serially diluted compounds (0.003–100 μM) were added to the cells. Following 2 h of incubation with compounds, cells were treated for 24 h with either 20% FBS (Thermo Fisher Scientific) ('serum-stimulated') or without ('non-serum-stimulated') containing growth medium 1B. Cells were then lysed and analyzed using a luciferase assay system (Promega) according to the manufacturer's protocol. Luminescence was measured using a BioTek Cytation 3 reader. In parallel, cell viability assays in AP1-luc HEK293 cells were carried out to gauge compound toxicity. Cells were seeded and treated similarly to the AP1 reporter assays. After serum stimulation, cells were analyzed using the CellTiter-Glo luminescent cell viability assay (Promega), according to the manufacturer's protocol. Luminescence was measured using a BioTek Cytation 3 reader. All statistical tests were performed with GraphPad Prism v.9.0, (GraphPad Software). Results are represented as means ± standard error of the mean (SEM). Two-way analysis of variance (ANOVA) with a Tukey post-hoc test was carried out when multiple comparisons were evaluated. Values were considered to be significant at $^{*}P < 0.05$, $^{**}P < 0.01$, $^{***}P < 0.001$, $^{****}P < 0.0001$.

Toxicity assays in HMC3 and NPC cell lines

Human microglial clone 3 (HMC3) cells (ATCC CRL-3304) were seeded in a volume of 40 μl at 3,850 cells/well on 384-well plates (Corning, cat. 3912). The particular HMC3 clone used was engineered through CRISPR gene editing to express a luciferase reporter for the GRN gene although measures of GRN expression were not included in the present study. HMC3 cells were cultured in 90% Eagle minimum essential medium (EMEM) with Earl's balanced salt solution (EBSS) and L-glutamine (Lonza), 10% fetal bovine serum (FBS, Sigma), 1% penicillin–streptomycin (Gibco) and 1 mM sodium pyruvate (Sigma)) and allowed to proliferate at 37 °C with 5% CO_2. After 24 h, compounds were dispensed to inner wells to indicated concentrations using a Tecan D300e dispenser, with all wells DMSO-normalized to 0.60%. After the indicated time points (24 or 72 h), plates were removed from the incubator, and 10 μl of medium in each well was replaced with 30 μl of CT-Glo 2.0 reagent (Promega G9242). Plates were allowed to nutate at room temperature for 15 min before reading luminescence using a PerkinElmer EnVision 2103 Multilabel Reader.

Generation of an expandable neural progenitor cell line (NPC; 8330-8 RC1) through an induced pluripotent stem cell (iPSC) intermediate from human fibroblasts (GM8330, Coriell Institute for Medical Research, Camden, NJ) was previously described (42). NPCs were seeded at 30 000 cells/well in a volume of 200 μl on 96-well plates (Corning, cat. 3901) that were previously coated sequentially with 20 μg/ml poly-ornithine (Sigma, P3655) in water for 3 h at 37°C with 5% CO_2 and then 5 μg/ml laminin (Sigma, L2020) diluted in PBS overnight at 37°C with 5% CO_2. NPCs were cultured in Dulbecco's modified Eagle's medium (DMEM, 68%, Gibco) with nutrient supplements Ham's F-12 (29%, Thermo Fisher Scientific) and B27 (2%, Gibco), and 1% penicillin-streptomycin (Gibco), supplemented with epidermal growth factor (EGF, 20 ng/ml, Sigma), basic fibroblast growth factor (bFGF, 20 ng/ml, Reprocell), and heparin (5 μg/ml, Sigma) and allowed to proliferate at 37°C with 5% CO_2. After 48 h of proliferation, compounds were dispensed to inner wells to indicated concentrations using a Tecan D300e dispenser, with all wells DMSO-normalized to 0.13%. After the indicated time points (24 or 72 h), plates were removed from the incubator, aspirated, and to each well was added 50 μl phosphate-buffered saline (PBS) followed by 50 μl of CT-Glo 2.0 reagent (Promega G9242). Plates were allowed to nutate at room temperature for 15 min before reading luminescence using a PerkinElmer EnVision 2103 Multilabel Reader.

Reporter assays ΔFOSB $Cys^{172}Trp$

Neuro2a cells (N2a; American Type Culture Collection) were cultured in EMEM (ATCC; Manassas, VA) supplemented with 10% heat-inactivated FBS (ATCC; Manassas, VA) and 5% penicillin/streptomycin (Sigma; St. Louis) in a 5% CO_2 humidified atmosphere at 37°C. Cells were seeded onto 12-well plates to reach 90–100% confluence the next day and were then transfected with the desired plasmids using Lipofectamine (Invitrogen; Waltham, MA). A total of 1000 ng of DNA was transfected per well. ΔFOSB and JUND cDNAs subcloned into a pcDNA3.1 vector (Invitrogen; Carlsbad. CA) were used, as previously described (43). Cells were transiently co-transfected with a combination of 4× AP-1/RSV-Luc plasmid and pcDNA3.1 containing wild-type or mutant ΔFOSB with or without JUND. The amount of wild-type or mutant ΔFOSB plasmid was titrated based on the protein expression quantified by western blot analysis to ensure that the total expression of each variant was the same. Approximately 48 h post-transfection, cells were washed twice with 1 ml PBS, and whole-cell lysates were prepared using 150 μl lysis buffer provided with the ONE-Glo Luciferase Assay System (Promega; Madison, WI). 50 μl of the lysate was removed for western blot analysis. The remaining lysates were incubated on ice for 5 min, and the luciferase activity (luminescence) present in each sample was assayed according to the manufacturer's instructions. The luminescence of each sample was measured in triplicate using a TD-20/20

luminometer (Turner Biosystems) with a 2 s premeasurement delay and a 1 s measurement period. Even though ΔFOSB plasmid transfection amounts were adjusted to express equal amounts of protein for each variant, the final luminescence signal was normalized to total ΔFOSB expression as assessed by post hoc Western blot of every replicate to eliminate variation due to pipetting errors or well-to-well differences in transfection efficiency. Separate measurements from three wells were averaged to obtain a single data point for each experiment, and the experiment was repeated at least three times to generate the presented data.

RESULTS

Structural insight into the redox switch of ΔFOSB/JUND

To understand how the redox switch in ΔFOSB/JUND regulates DNA binding and how ΔFOSB/JUND forms a target that can be regulated by small-molecule modulators, we first determined the X-ray crystal structure of ΔFOSB/JUND bZIP in the reduced, DNA-free form (ΔFOSB/JUND^{red}) using diffraction data to 2.4 Å (Figure 2A, Table 1). This structure visualizes the key missing state of a trio that includes the ΔFOSB/JUND bZIP in the oxidized, DNA-binding-compromised form (ΔFOSB/JUNDox; PDB ID: 5VPC) and in complex with DNA (ΔFOSB/JUND^{DNA}; PDB ID: 5VPE), both of which we determined previously. These three structures together reveal crucial insights into the molecular underpinnings of the redox switch (Figure 2B–D). In the reduced, DNA-free form, both ΔFOSB and JUND assume essentially all-helical structures throughout, despite lacking DNA or being stabilized by a disulfide bond like the oxidized form (Figure 2A). The N-terminal DNA-binding regions are splayed apart evenly from the central dimer axis with the putative redox-switch cysteines ΔFOSB Cys^{172} and JUND Cys^{285} separated by ∼9 Å (Figure 2A). The C-terminal leucine zippers in both bZIP subunits form the typical coiled-coil superstructure. By contrast, in the oxidized state, ΔFOSB/JUND^{ox}, a disulfide bond is formed between the cysteines, which is accompanied by a sharp kink in the ΔFOSB Arg^{175}-Arg^{176} region that redirects the otherwise all-helical structure (Figure 2B and C). Comparison of ΔFOSB/JUND^{red} with the DNA-bound form (ΔFOSB/JUND^{DNA}), reveals that the DNA-binding regions can scissor to engage the major groove of the AP1 consensus sequence, displacing in opposite directions along the DNA strand through a rotation of about 45 degrees anchored around the hinge points ΔFOSB Ala^{185} and JUND Glu^{298}, respectively (Figure 2D). In the DNA-bound state, the putative redox-switch cysteines are separated by ∼14 Å. Thus, the major structural transitions that accompany activation of the redox switch, i.e. disulfide-bond formation, occur only in ΔFOSB bZIP, while the JUND bZIP structure remains largely unchanged (Figure 2E). Our data suggest that the ΔFOSB/JUND bZIP houses ordered DNA-binding motifs that are under the control of a redox switch and that together form a compound-binding region that can be leveraged for drug discovery.

Screening for compounds that target the redox switch of ΔFOSB

To identify small-molecule ligands that target the redox switch in ΔFOSB, we screened the 'Cysteine-focused Covalent Fragments' library (Enamine, Monmouth Jct., NJ) composed of 3200 compounds selected for their ability to covalently bind to cysteine residues. The library included acrylates and their active analogs, α,β-unsaturated sulfones and sulfonamides, activated terminal acetylenes, activated cyano-groups, aliphatic thiols, epoxides, lactones, lactams, and sulfonyl fluorides. We used a fluorescence polarization (FP) assay that monitors the binding of a TAMRA-labeled oligonucleotide (TMR-*cdk5*) to recombinant ΔFOSB/JUND heterodimers ('ΔFOSB/JUND') or ΔFOSB homomers ('ΔFOSB') to screen for compounds that disrupt DNA binding (30). For ΔFOSB/JUND, 16 compounds inhibited DNA binding by ≥50% at a concentration of 50 μM, with seven compounds inhibiting DNA binding by ≥75%. Similarly, for ΔFOSB, 10 compounds inhibited DNA binding by ≥50%, with six compounds inhibiting DNA binding by ≥75%. Only one of these compounds is unique for ΔFOSB, with the others inhibiting DNA binding to both ΔFOSB/JUND and ΔFOSB. In FP-based dose-response curves (FP-DRCs) three out of the combined 17 (16 + 1) were validated as robustly active. They contain one of two distinct chemically reactive groups: Group A consists of α-haloketones with a reactive chloroacetyl group (Figure 3A), and Group B contains an acrylamide reactive group (Figure 3B). We also acquired several similar compounds with the same reactive groups as additional 'analogs' to further probe the selectivity of the hit compounds (Figure 3A and B). The remaining ten compounds were inactive in this assay at <100 μM, and four interfered with the assay by impacting the FP signal of the TMR-*cdk5* oligo alone. The FP-DRC data could be fitted as 'regular' IC_{50} values, suggesting that the initial binding phase within the timeframe of our experiments is a reversible association step that only later is followed by irreversible covalent attachment of the compounds to the reactive cysteines. In Group A, Z2159931480 disrupted the binding of ΔFOSB/JUND and ΔFOSB to TMR-*cdk5* with IC_{50} values of 22.3 ± 1.9 μM and 27.4 ± 0.1 μM, respectively, while the smaller analogs 2196-99-8 and 456-04-2 (compound codes derived from their CAS numbers) did not affect DNA binding up to 200 μM (Figure 3D, E, and Supplementary Figure S1). We confirmed the ability of Z2159931480 to disrupt binding of DNA to ΔFOSB/JUND using electrophoretic mobility assays (EMSAs) (Figure 3D). In Group B, Z3247353427 disrupted the binding of ΔFOSB/JUND and ΔFOSBto TMR-*cdk5* with IC_{50} values of 22.5 ± 4.6 μM and 29.0 ± 0.6 μM, respectively (Figure 3E). Z2492395544 was less potent with IC_{50} values of 71.4 ± 3.1 μM and 96.8 ± 7.2 μM for ΔFOSB/JUND and ΔFOSB, respectively, while 1183031-77-7 did not disrupt DNA binding (up to ∼200 μM) (Figure 3E and Supplementary Figure S1). We also confirmed the ability of Z3247353427 to disrupt the binding of ΔFOSB/JUND to DNA using EMSA (Figure 3E).

We next assessed the binding of the validated compounds to the ΔFOSB/JUND bZIP using liquid chromatography-

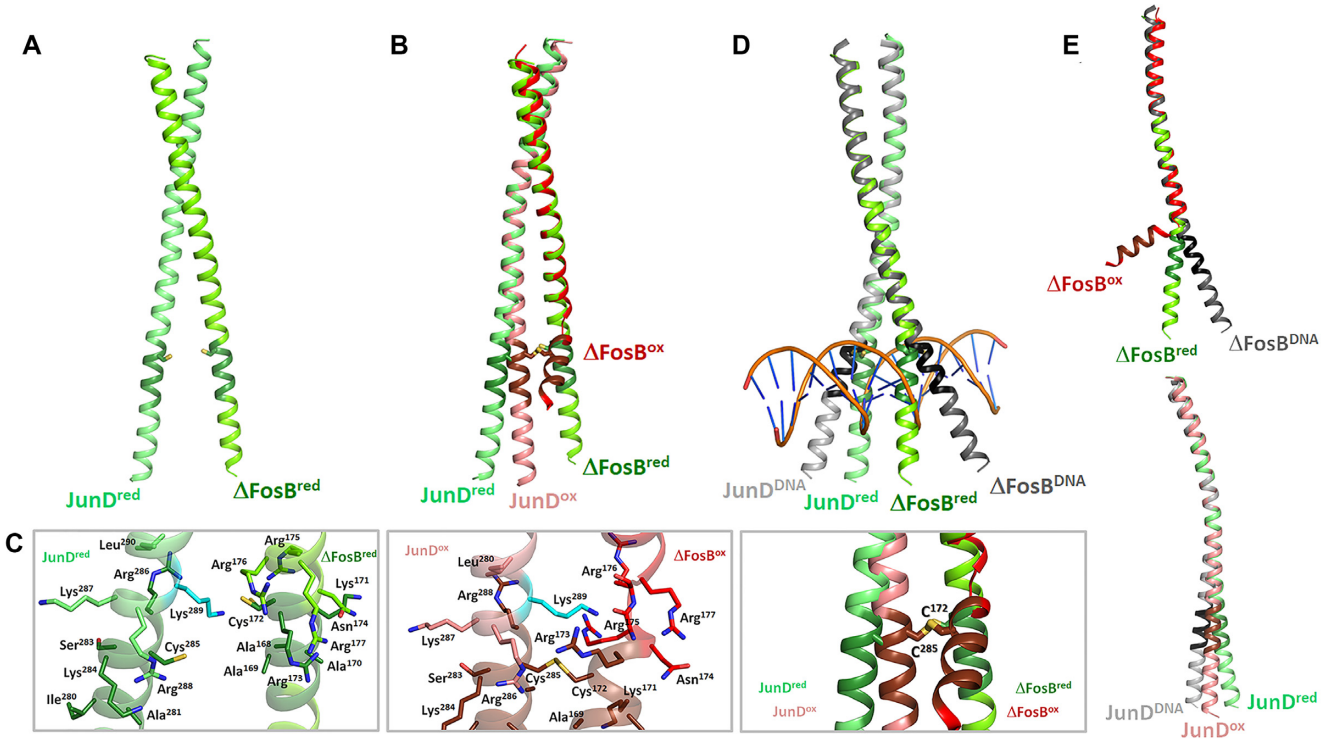

Figure 2. Three-dimensional structure of ΔFOSB/JUND^{red}. (**A**) Crystal structure of the ΔFOSB/JUND bZIP under reducing conditions (ΔFOSB/JUND^{red}). (**B**) Superposition of ΔFOSB/JUND^{red} (green) and ΔFOSB/JUND^{ox} (red; PDB ID: 5VPC) using the leucine zipper residues JUND (Asn^{301}-Gln^{317}). (**C**) Close-up views of ΔFOSB/JUND^{red} (left), ΔFOSB/JUND^{ox} (middle), and the superposition of ΔFOSB/JUND^{red} (green) and ΔFOSB/JUND^{ox} (red) (right). (**D**) Superposition of ΔFOSB/JUND^{red} and ΔFOSB/JUND^{DNA} (PDB ID 5VPE) using the leucine zipper residues JUND (Asn^{301}-Gln^{317}). (**E**) Comparison of the isolated ΔFOSB bZIP subunits (top) and JUND bZIP subunits (bottom) from ΔFOSB/JUND^{red} (green), ΔFOSB/JUND^{ox} (red), and ΔFOSB/JUND^{DNA} (grey) using the leucine zipper residues JUND (Asn^{301}-Gln^{317}) to superimpose the ΔFOSB/JUND assemblies. For (A)–(E), the DNA-binding motifs (ΔFOSB Asn^{165}-Arg^{173} and JUND Asn^{278}- Arg^{286}) are shown in a darker color, and ΔFOSB Cys^{172} and JUND Cys^{285} are shown in yellow. Side chains are shown in half-bond colors: non-carbon atoms in red (oxygen), blue (nitrogen), and yellow (sulfur).

mass spectrometry (LC-MS). Group A compounds (Z2159931480, 2196-99-8 and 456-04-02) bind to both the ΔFOSB and JUND bZIPs with each subunit binding one compound molecule (Figure 4A–C, Supplementary Table S1). The major species observed are the ΔFOSB and JUND bZIP subunits containing a compound moiety each that has lost an H and a Cl atom indicating covalent addition to the protein (observed at mass 8447.427 Da for ΔFOSB bZIP and 8167.660 Da for JUND bZIP, respectively). For compound Z2159931480, a significant percentage of ΔFOSB and JUND (4–7%) was also found associated with an intact Z2159931480 molecule observed at 8483.395 Da and 8203.636 Da, respectively (i.e. no loss of the H and Cl atoms, Figure 4C, Supplementary Table S1), suggesting that the compound can bind to the protein stably (within the timeframe of the MS experiment) before a covalent bond is formed, an important mechanistic insight. By contrast, Group B compounds were not efficiently observed in a covalently bound form within the timeframe of the experiment, except for 1183031-77-7 where small amounts of protein:compound complex were detected (<2%) (Supplementary Table S1). Finally, using peptide mapping and tandem MS, we identified the y2 fragment ion for ΔFOSB Cys^{172} and JUND Cys^{285} (Δ mass 307.0508 Da) revealing that each bind to a Z2159931480 molecule (Figure 4D and E). Thus, our screening cascade successfully identified compounds that target the redox-switch residues ΔFOSB Cys^{172} and JUND Cys^{285}.

Molecular insight into compounds targeting the redox switch of ΔFOSB/JUND

To elucidate the mechanism of action of compounds targeting the redox switch, we determined the X-ray crystal structure of ΔFOSB/JUND bZIP in complex with Z2159931480 (ΔFOSB/JUND^{cmpd}) using diffraction data to 3.2 Å (Figure 5A, Table 1). While the determination and refinement of this structure were complicated by severely anisotropic X-ray diffraction of our crystals, the electron density unambiguously indicates that ΔFOSB Cys^{172} is covalently modified and that a Z2159931480 moiety fits the extra electron density attached to ΔFOSB Cys^{172} (Figure 5B). Z2159931480 fits in between the helical DNA-binding motifs of ΔFOSB and JUND at the fulcrum of the bZIP dimer where the leucine zipper ends and the DNA-binding motifs splay apart (Figure 5C). Z2159931480 packs within 5 Å against the side chains of JUND Ala^{282}, Arg^{286}, and Lys^{289}, and ΔFOSB Ala^{169}, as well as against the main chain of ΔFOSB Arg^{173} (Figure 5C). The JUND Arg^{286} guanidino group forms a π−π stacking interaction with the central benzofuran-3(2H)-one moiety in Z2159931480. The attachment of Z2159931480 does not distort the over-

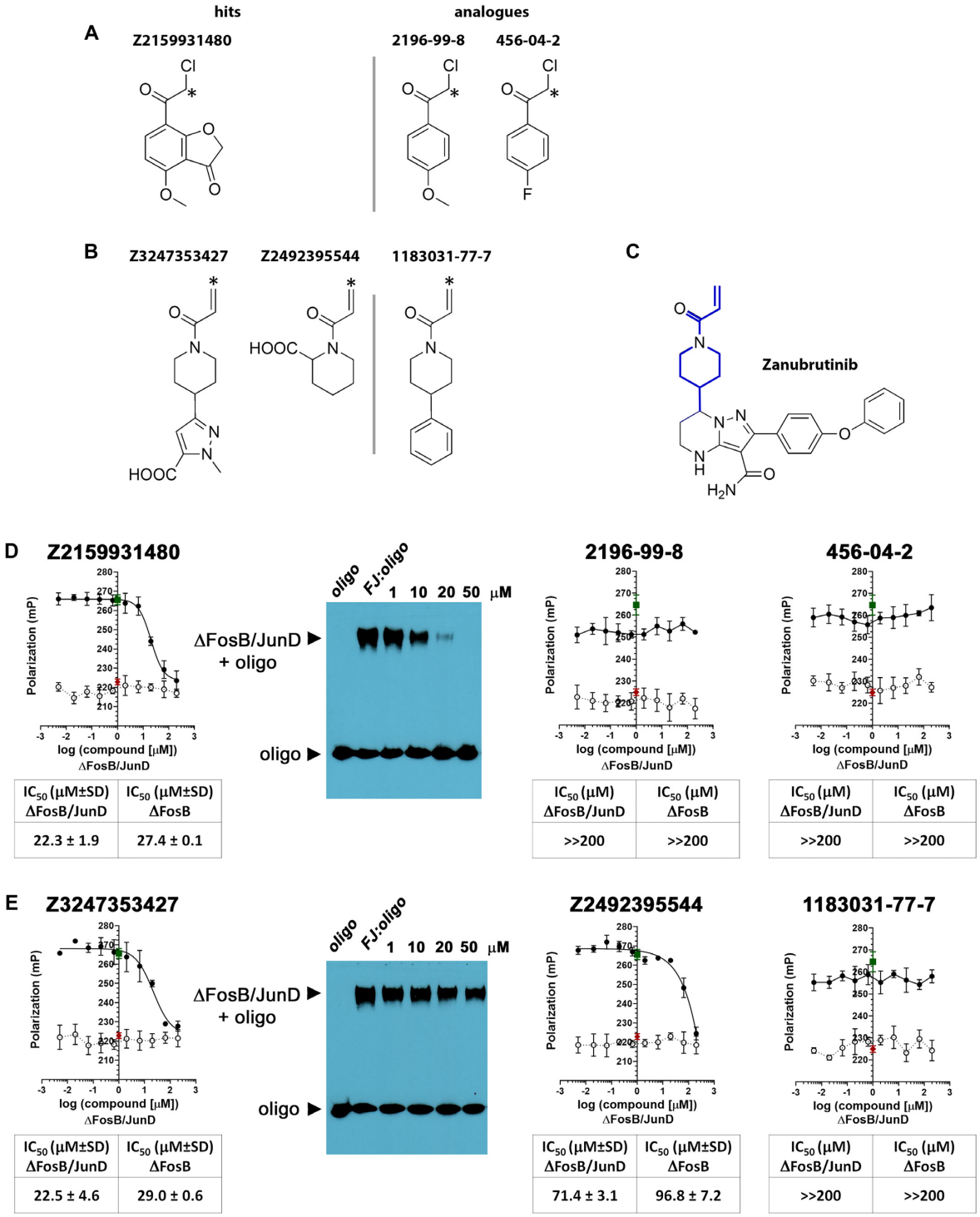

Figure 3. Compounds targeting the ΔFOSB redox switch. (**A**) Group A compounds contain an α-haloketone reactive group. (**B**) Group B compounds contain an acrylamide reactive group. (**C**) zanubrutinib, an unrelated FDA-approved Bruton's tyrosine kinase inhibitor contains a similar acrylamide warhead and piperidine-ring as the Group B compound Z3247353427 (in blue bold lines). *denotes the atom that forms the covalent link to a cysteine Sγ atom in a protein. (**D**) Group A compounds assessed in fluorescence polarization (FP)-based dose-response assays (shown for ΔFOSB/JUND) and an electrophoretic mobility shift assay (EMSA). (**E**) Group B compounds assessed in FP-based dose-response assays (shown for ΔFOSB/JUND) and EMSA. For (D) and (E), compounds were tested by incubating 25 nM TMR-*cdk5* oligo with increasing amounts of compound (0–200 μM) in presence of 280 nM ΔFOSB/JUND full-length protein (●) or in absence of protein (o). As controls, the FP readings for the *cdk5* oligo alone (♦, equivalent to '100%-inhibition') and ΔFOSB/JUND + *cdk5* oligo (■, equivalent to '0%-inhibition'), respectively, are indicated. Error bars indicate the standard deviation (SD) of four replicates for each data point. IC50 values are averaged over two independent experiments. The compounds were also tested against ΔFOSB full-length protein (see Supplement). Compound activities for Z2159931480 and Z3247353427 were orthogonally validated using EMSAs by incubating ΔFOSB/JUND with a biotinylated-*cdk5* oligo (BIO-*cdk5*) and increasing amounts of compound (1, 10, 20 and 50 μM). BIO-*cdk5* alone ('oligo') and the starting amount of ΔFOSB/JUND:BIO-*cdk5* complex in the absence of compound ('FJ:oligo') are shown as well.

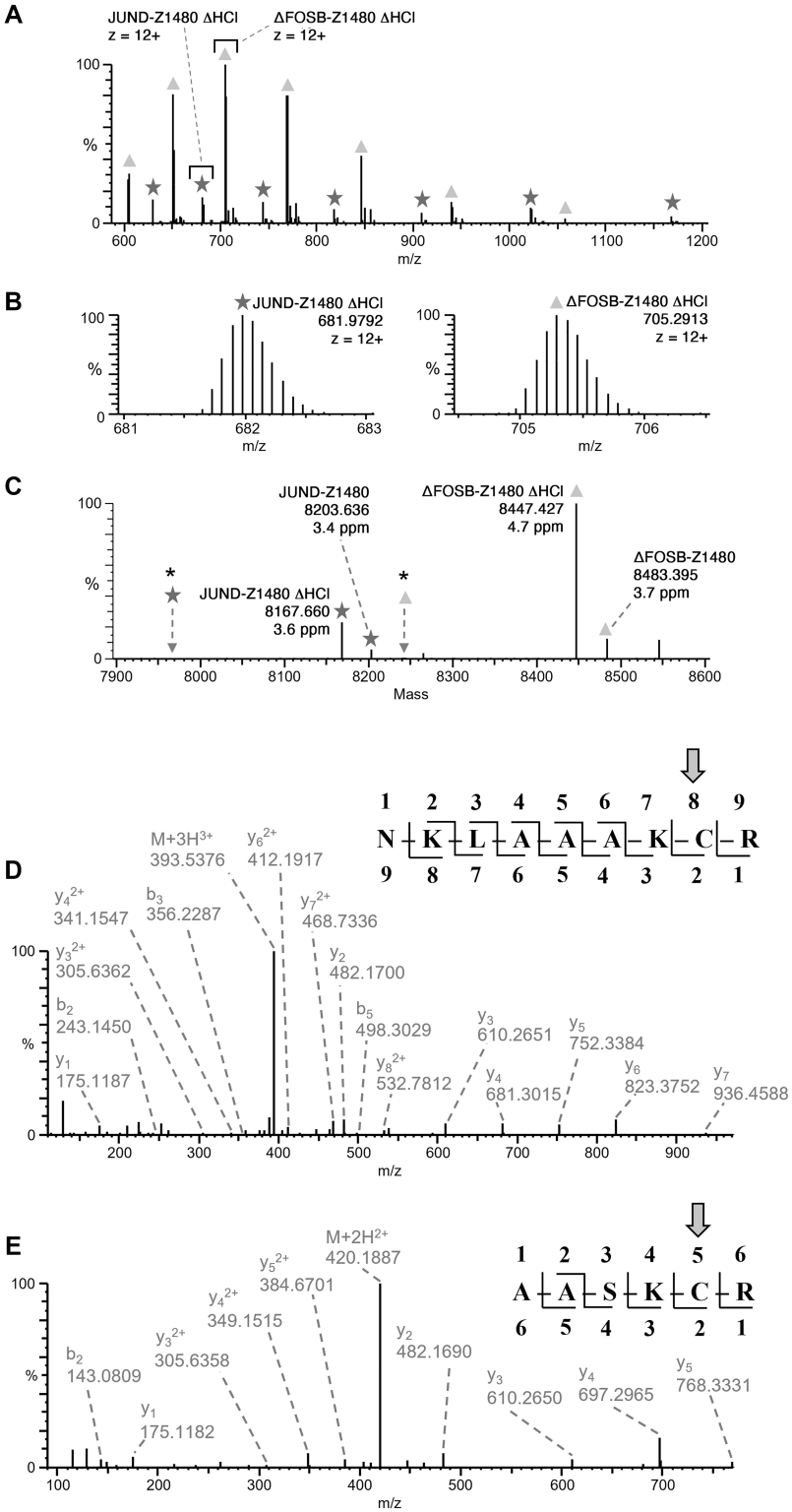

Figure 4. Mass spectrometric (MS) analysis of the ΔFOSB/JUND bZIP + Z2159931480 complex. MS reveals the covalent addition of one Z2159931480 molecule per subunit accompanied by the loss of one H- and one Cl-atom. (**A**) MS1 spectrum showing the charge state profile of co-eluting compound-treated ΔFOSB (indicated by triangle) and JUND (indicated by star). (**B**) Zoom-in of the MS1 spectrum from bracketed regions shown in panel (A) showing the 9 + charge states of ΔFOSB and JUND. (**C**) Sliding Window Xtract Deconvolution spectrum of compound-treated ΔFOSB and JUND reveals accurate masses (3 - 5 ppm mass error) corresponding to the addition of one Z2159931480 molecule and loss of HCl. Asterisks indicate the expected mass of unmodified forms of ΔFOSB and JUND that were not observed. (**D**) MS/MS spectra identify the compound-treated ΔFOSB tryptic peptide NKLAAAKCR and Cys^{172} as the site of covalent modification by Z2159931480. (**E**) MS/MS spectra identify the JUND semi-tryptic peptide AASKCR and JUND Cys^{285} as the site of covalent modification by Z2159931480. Complete coverage was obtained for the C-terminal y-series fragment ions in (D) and (E), revealing the cysteines as the specific sites for modification by Z2159931480.

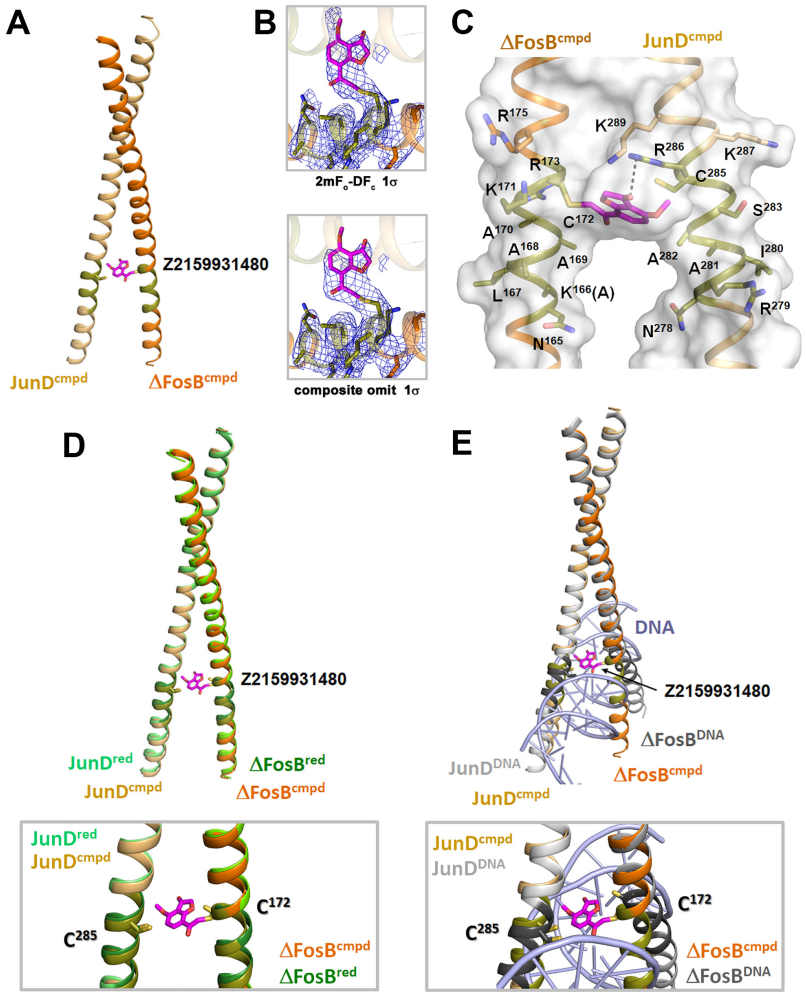

Figure 5. Three-dimensional structure of ΔFOSB/JUND^{cmpd}. (**A**) Crystal structure of the ΔFOSB/JUND bZIP + Z2159931480 (ΔFOSB/JUND^{cmpd}) using diffraction data to 3.2 Å. (**B**) SigmaA-weighted $2mF_o - DF_c$ electron density map (top); composite omit map for the region surrounding the ΔFOSB Cys^{172} + Z2159931480 moiety (bottom). Both maps are contoured at 1 σ. (**C**) Close-up of the Z2159931480 molecule bound to ΔFOSB Cys^{172} at the fulcrum of the ΔFOSB/JUND bZIP forceps (molecular surface shown in grey). (**D**) Superposition of ΔFOSB/JUND^{cmpd} (orange) and ΔFOSB/JUND^{red} (green) using the leucine zipper residues JUND (Asn^{301}-Gln^{317}) (top). Zoom-in view (bottom). (**E**) Superposition of ΔFOSB/JUND^{cmpd} (orange) and ΔFOSB/JUND^{DNA} (grey, PDB ID 5VPE) using the leucine zipper residues JUND (Asn^{301}-Gln^{317}) (top). Zoom-in view (bottom). For (A)–(E), the DNA-binding motifs (ΔFOSB Asn^{165}-Arg^{173} and JUND Asn^{278}- Arg^{286}) are shown in darker colors, and ΔFOSB Cys^{172} and JUND Cys^{285} are shown in yellow. The Z2159931480 molecule is shown in magenta. Side chains are shown in half-bond colors: non-carbon atoms in red (oxygen), blue (nitrogen) and yellow (sulfur).

all bZIP structure or the curvature of the helices compared with the compound-free form (Figure 5D). In our crystal form, neighboring molecules do not contact the compound directly, though they may influence the region near the redox switch (Supplementary Figure S2a and b). For example, the carboxyl terminus of a symmetry-related JUND bZIP (Val^{332}) docks near JUND Arg^{286} and Lys^{289}, residues that participate in forming the bottom of the crevasse that Z2159931480 binds into, balancing the electrostatic charges in this region (Supplementary Figure S2c, contact #3). In the DNA-bound form ΔFOSB/JUND^{DNA}, these two positively charged side chains are also in close proximity to each other, but they are stabilized by a phosphate ion (24). Strikingly, while JUND Cys^{285} is well-resolved in the electron density for ΔFOSB/JUND^{cmpd}, there is no extra electron density to indicate a bound Z2159931480 molecule, despite its unambiguous presence by mass spectrometry (Figure 2).

Due to the two-fold symmetry of the ΔFOSB/JUND structure, an analogous binding site to accommodate JUND Cys^{285} + Z2159931480 would likely involve ΔFOSB Ala^{169} (equivalent to JUND Ala^{282}), ΔFOSB Arg^{173} (equivalent to JUND Arg^{286}), and ΔFOSB Arg^{176} (equivalent to JUND Lys^{289}). Unlike the equivalent residues in JUND, however, these ΔFOSB residues do not form a platform onto which a compound bound to JUND Cys^{285} can dock, because ΔFOSB Arg^{173} is incorporated in a ladder of salt bridges with a neighboring ΔFOSB molecule (instead of its partner JUND) that likely stabilizes the crystal packing (Supplementary Figure S2c, contact #1). Hence, this particular crystal packing likely selects for heterodimers that are modified only at ΔFOSB Cys^{172} as it may be incompatible with an additional modification at JUND Cys^{285}. Nevertheless, the ΔFOSB/JUND^{cmpd} structure reveals important mechanistic insights into how bound com-

pounds disrupt DNA binding: based on a superposition with ΔFOSB/JUND^{DNA}, the Z2159931480 molecule attached to ΔFOSB Cys^{172} cannot be accommodated without directly clashing with DNA (Figure 5E). Taken together, our results indicate that a deep pocket at the fulcrum of the bZIP forceps housing the redox-switch residues can be targeted by cysteine-focused compounds, suggesting a strategy for drug discovery targeting ΔFOSB and other AP1 transcription factors.

Cellular action of compounds targeting the redox switch of ΔFOSB/JUND

Given their broad potential for chemical reactivity, we evaluated the toxicity of Group A and Group B compounds using an ATP-based cell viability assay in two different human cell lines. This was a crucial step to determine whether the biological effect of the compounds, i.e. their impact on gene expression, could be assessed in cells as well. In human brain microglia clone 3 (HMC3) cells, Group A compounds did not exhibit toxicity at 24 h (0–30 μM) and were reasonably tolerated even up to 72 h (at ∼11 μM, >75% cell viability for Z2159931480 and 2196-99-8, and 66% for 456–0402, respectively) (Figure 6A). Group B compounds were even better tolerated, with HMC3 cells showing no signs of toxicity up to 72 h (0–30 μM) (Figure 6B). Human induced pluripotent stem cell (iPSC)-derived neural progenitor cells (NPCs) were more sensitive to Group A compounds, tolerating doses up to 5 μM with >∼75% cell viability up to 72 h, except 456-0402 (67% at 24 h and 28% at 72 h, respectively) (Figure 6C). Like in HMC3 cells, the Group B compounds were very well tolerated by NPCs up to the maximum time interval and dose tested (72 h; 0–25 μM) (Figure 6D).

To determine the biological activity of our small-molecule modulators, we developed a cell-based reporter assay using a recombinant human embryonic kidney 293 (HEK293) cell line with an AP1-consensus-site-driven luciferase reporter stably integrated (AP1-luc HEK293, BPS Bioscience, USA). We applied a serum-starvation-stimulation protocol to induce the expression of AP1 transcription factors, which in turn would induce the expression of the AP1-luciferase reporter gene. We serum-starved cells for 24 h, followed by 24 h exposure to fetal bovine serum (FBS), which leads to the accumulation of ΔFOSB over FOSB or c-FOS, as was shown previously in PC12 cells (21,44) (Supplementary Figure S3). We validated our reporter assay using compound T5224, a known inhibitor of AP1 transcription factors with undetermined mode of interaction (45,46) (Supplementary Figure S4a), which revealed a ∼3x-fold dose-dependent decrease in AP1-driven luciferase signal in FBS-treated AP1-luc HEK293 cells, as expected (Figure 6E). We re-tested the toxicity of our compounds in the AP1-luc HEK293 cells under conditions mirroring our reporter assay. AP1-luc HEK293 cells were serum-starved, incubated with compounds for 2 h, and then stimulated with FBS to induce the expression of AP1 transcription factors. Group A compounds showed essentially no visible cell death up to 31.5 μM, and Group B compounds none up to 100 μM (Figure 6F). We recorded dose-response curves in our luciferase-reporter assay using 31.5 μM as the maximal dose for Group A compounds and 31.5 and 100 μM for Group B compounds (based on the cell viability studies in AP1-luc HEK293 cells) (Figure 6F). Unlike treatment with T5224, Group A compounds triggered a strong dose-dependent increase in AP1-driven luciferase signal, suggesting they have a potentiating effect on AP-1-driven gene expression (Figure 6G). In particular, compounds 2196-99-8 and 456-04-2 caused a ∼4-fold increase in luciferase signal compared to control, reaching a maximal effect by ∼10 μM, though toxicity concerns limited the upper dose of Z2159931480 that could be tested. Group B compounds also triggered a dose-dependent increase in luciferase activity, albeit significantly smaller (<1.5-fold), compared to the control (Figure 6H). Although the potentiating effects of Group B compounds on reporter-gene expression were less strong, they were more potent than those in Group A, reaching their half-maximal effect at doses below 0.3 μM (EC_{50} 0.26 μM for Z3247353427 and EC_{50} 0.11 μM for Z2492395544). As a control, adding the compounds to AP1-luc HEK293 cells when the FBS treatment was omitted (i.e. no induction of AP1 proteins) did not alter the luciferase activity significantly as shown for representative compounds (Z2159931480 and Z3247353427) (Figure 6G and H, left insets). Likewise, all Group A compounds and two out of three Group B compounds, triggered a much higher potentiating effect on reporter gene expression when they were administered together with FBS stimulation, suggesting that these compounds work on AP1 transcription factors that are induced by FBS stimulation (Figure 6G and H, right insets with bar graphs). Overall, our data suggest that Group A and Group B compounds are well tolerated in cells (except 456-0402), despite having cysteine-reactive groups. Also, both scaffolds have a net potentiating effect on AP1-mediated gene expression in cell-based assays (in contrast to T5224, which inhibits the reporter gene expression), though Group A and Group B compounds differ in the extent to which they induce luciferase expression; in addition, both scaffolds are much more active in cells than in biochemical assays (see next section and the Discussion).

Mechanism of action of Group A and Group B compounds

We investigated the mechanism of action of our compounds further with a series of targeted studies (Figure 7). First, we tested the ability of the compounds to disrupt the binding of ΔFOSB Cys^{172}Ser/JUND heterodimers to DNA in FP assays to assess whether covalent binding was essential for their action. Given that the compounds are also active against wild-type ΔFOSB homomers (Figure 3 and Supplementary Figure S1), we also tested the compounds against ΔFOSB Cys^{172}Ser homomers, which are devoid of any redox-switch cysteines. Compounds Z2159931480 (Group A), Z3247353427 (Group B), and T5224 (which does not covalently attach) disrupt the binding of DNA to ΔFOSB Cys^{172}Ser/JUND heterodimers and ΔFOSB Cys^{172}Ser homomers similarly well as to the wild-type species (Figure 7a and Supplementary Figure S4). These results indicate that Z2159931480 and Z3247353427 are able to bind to a preformed site (or induce one) in the wild-type proteins and exert their disruptive effect on DNA binding without requiring covalent attachment to the redox-switch cysteines (just like T5224). Covalent modification then likely occurs over

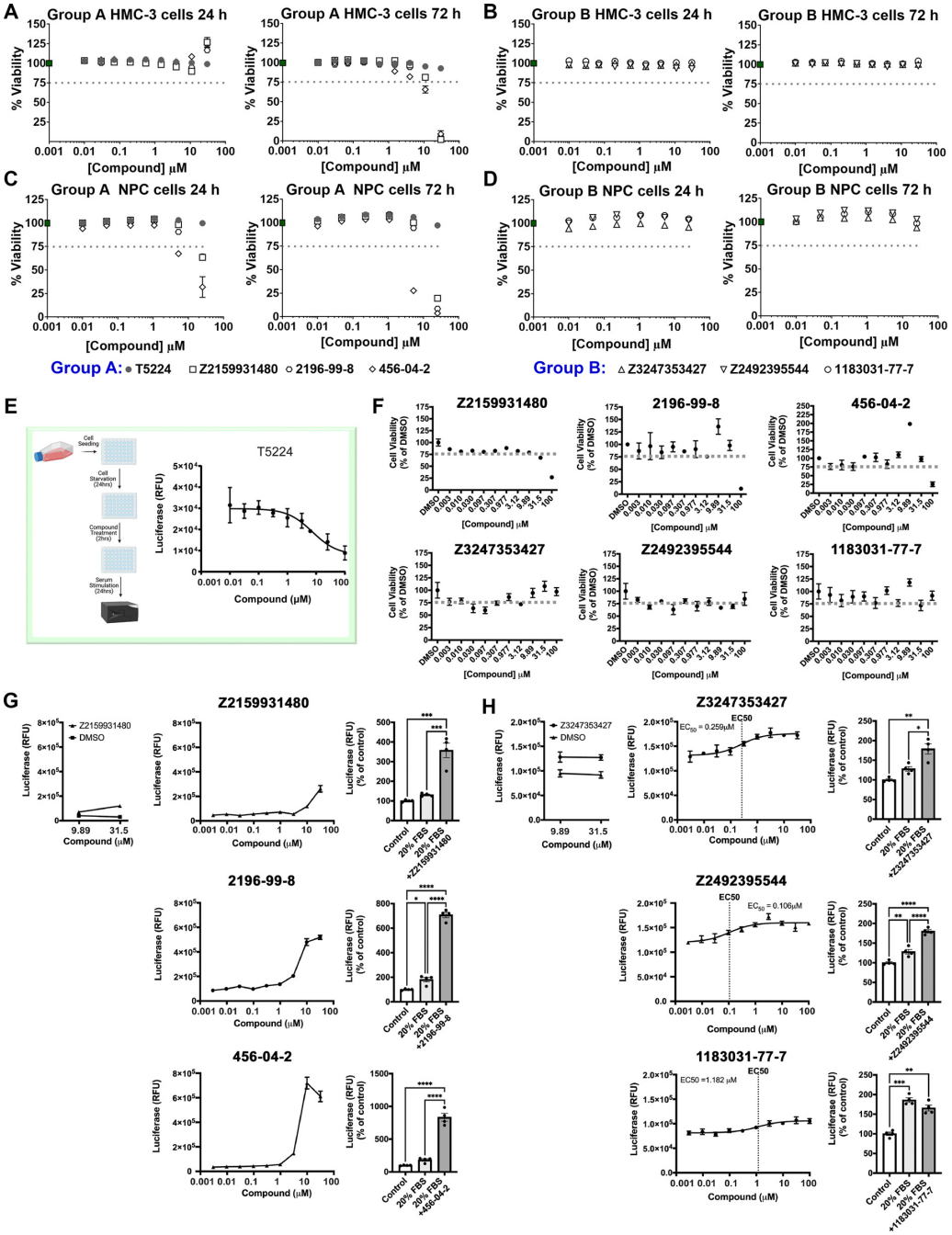

Figure 6. Cell-based assays for compound testing. (**A**) Impact of Group A compounds (0–30 μM; 24 h and 72 h) on HMC3 cell viability. (**B**) Impact of Group B compounds (0–30 μM; 24 h and 72 h) on HMC3 cell viability. (**C**) Impact of Group A compounds (0–25 μM; 24 h and 72 h) on NPC viability. **d**) Impact of Group B compounds (0–25 μM; 24 h and 72 h) on NPC viability. For (A), (B), (C) and (D), cell viabilities are normalized to the negative control containing 0.60% DMSO and no compound (green square ■). Grey dotted lines indicate 75% cell viability. (**E**) AP-1 reporter assay and cell viability assay developed to test the biological activity of compounds targeting ΔFOSB. The known AP1 inhibitor, T5224, was used as a positive control to measure the dose-dependent decrease in AP1-driven luciferase expression following treatment of AP1-luc-HEK293 cells with T5524 (0–100 μM). Data represent the mean ± SEM (standard error of the mean). (**F**) Impact of serially diluted compounds (0.003–100 μM) on the viability of AP1-luc HEK293 cells. Cell viabilities are normalized to the negative control containing no compound but 0.5% DMSO. Grey dotted lines indicate 75% cell viability. (**G**) Impact of Group A compounds on AP1-driven luciferase activity in AP1-luc-HEK293 cells (0–30 μM). Dose-dependent transactivation of the AP1-driven luciferase reporter is monitored as the change in luciferase signal and expressed as relative luciferase fluorescence units (RFU). The AP1 luciferase activity induced by Z2159931480 (9.9 and 31.5 μM) or 0.5% DMSO in non-serum treated AP1-luc HEK293 cells (i.e. low, or basal, levels of AP1 proteins expressed) is shown as a measure of off-target effects (left inset). In addition, bar graphs (right inset) show the fold change in luciferase signal following 0% FBS ('control'), 20% FBS treatment, or 20% FBS + compound (highest dose, 31.5 μM) expressed as a percentage of the 'control' non-serum treated AP1-luc HEK293 cells. (**H**) Impact of Group B compounds on AP1-driven luciferase activity in AP1-luc-HEK293 cells (0–31.5 or 0–100 μM). Data were fitted using a 3-parameter log-logistic function. Analogous controls were carried out for Group B compounds as described in (**G**). For (**G**) and (**H**), data represent the mean ± SEM ($n = 4$). $^{*}P < 0.05$, $^{**}P < 0.01$, $^{***}P < 0.001$, $^{****}P < 0.0001$ by two-way analysis of variance (ANOVA) with post-hoc analysis by Tukey's multiple comparison.

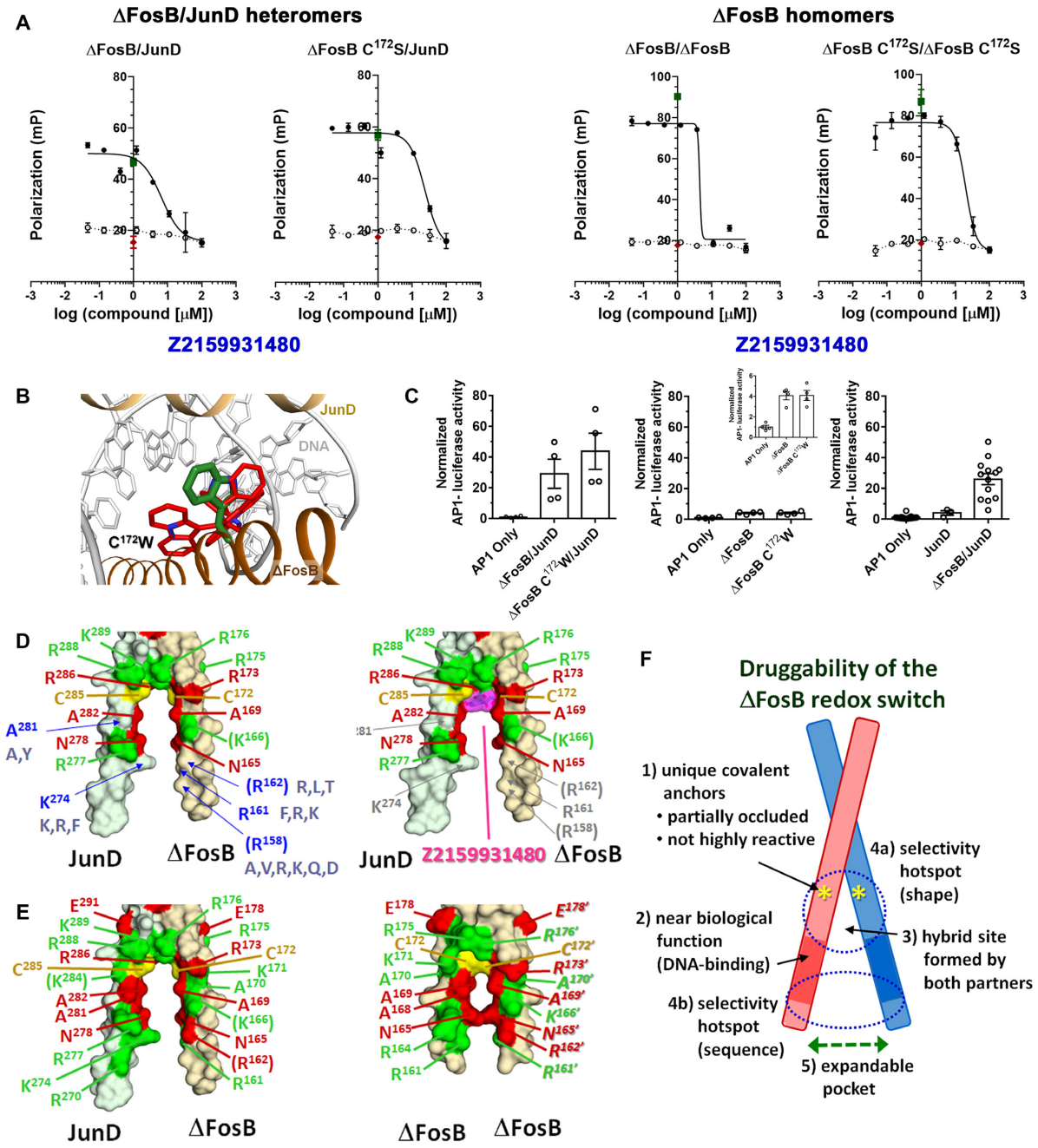

Figure 7. Mechanism of action of redox-switch-targeting compounds. (**A**) Z2159931480 assessed against full-length ΔFOSB/JUND, ΔFOSB Cys^{172}Ser/JUND, ΔFOSB/ΔFOSB, and ΔFOSB Cys^{172}Ser/ΔFOSB Cys^{172}Ser in FP-based dose-response assays. Compounds were tested by incubating 50 nM TMR-*cdk5* oligo at increasing amounts of compound (0–200 μM) in presence of 280 nM ΔFOSB/JUND full-length protein or mutant (●) or in absence of protein (o). The controls, '100%-inhibition' i.e. oligonucleotide alone (♦) and '0%-inhibition', i.e. ΔFOSB/JUND + *cdk5* oligo (■) are indicated. Error bars indicate the standard deviation of three independent data points. The compounds were tested against 280 nM ΔFOSB full-length protein or mutant. (**B**) Possible rotamer conformations of ΔFOSB Cys^{172}Trp modeled using the ΔFOSB/JUND^{red} bZIP structure. The red rotamers undergo steric clashes with protein and/or DNA rendering them unfavorable, the green one does not. (**C**) ΔFOSB Cys^{172}Trp/JUND heterodimers increase the transcription of an AP1-luciferase reporter at least as effectively as ΔFOSB/JUND heterodimers in cultured Neuro2A cells (left). Likewise, ΔFOSB Cys^{172}Trp homomers are as active as ΔFOSB homomers in regulating the AP1-luciferase reporter (middle). For comparison, the abilities of JUND homodimers versus ΔFOSB/JUND heterodimers to regulate the AP1-luciferase reporter are shown as well (right). Error bars represent mean ± SEM (standard error of the mean). (**D**) Sequence conservation of 29 human bZIP-containing proteins mapped onto the molecular surface of the ΔFOSB/JUND^{red} bZIP (left) and ΔFOSB/JUND^{cmpd} bZIP with Z2159931480 bound (right). Color-coding: red, conserved; green, semi-conserved; yellow, redox-switch cysteines. Residues with disordered side chains (not included in the surface calculation) are indicated in parentheses. Residues strategically located near the redox switch that diverge greatly are labeled in blue with other residues occurring across bZIPs listed in grey. (**E**) Sequence conservation of human FOS and JUN family members mapped onto the molecular surface of the ΔFOSB/JUND^{red} bZIP (left) and ΔFOSB homomers (PDB ID 6UCL). Color-coding: red, conserved; green, semi-conserved; yellow, redox switch. Residues with disordered side chains (not included in the surface calculation) are indicated in parentheses. In (D) and (E), the groups of semi-conserved residues were defined as follows: (R, K), (Q, E), (A, S, T) and (V, L). (**F**) Properties rendering the ΔFOSB redox switch druggable. ΔFOSB Cys^{172} and JUND Cys^{285} are represented by asterisks.

time after the initial, reversible protein:compound complex has formed. On the other hand, covalent modification of the redox-switch residues alone is not sufficient to disrupt DNA binding if the modifications are small, as exemplified by the Group A compounds. For instance, Z2159931480 disrupts DNA binding in FP assays, while the smaller analogs 2196-99-8 and 456-04-02 do not (Figure 3), yet all three compounds bind to ΔFOSB and JUND bZIP domains by MS (Supplementary Table S1). Small covalent modifications of the redox-switch cysteines can apparently be accommodated near the DNA-binding motifs without disrupting their ability to bind DNA. To mimic the effect of modifying ΔFOSB Cys^{172} with a small moiety, we mutated Cys^{172} to tryptophan. Replacing the cysteine side chain with that of tryptophan *in silico* in the ΔFOSB/$JUND^{DNA}$ crystal structure shows that the tryptophan side chain can assume a stable rotamer conformation that avoids clashes with DNA (Figure 7B). Indeed, purified recombinant ΔFOSB Cys^{172}Trp homomers bind DNA at least as well as the wild-type protein in FP assays (Supplementary Figure S5). In luciferase reporter assays in Neuro2a cells, mutant ΔFOSB Cys^{172}Trp induces transcription of a luciferase reporter gene to a similar extent as the wild-type counterpart, both as mutant ΔFOSB/JUND heterodimers and mutant ΔFOSB homomers (Figure 7C). Thus, covalent modification of redox-switch cysteines is neither sufficient nor necessary for compounds to disrupt DNB binding. This allows for the development of tools for discriminately modulating ΔFOSB/JUND activity: small compounds that covalently modify the redox-switch residues and that render ΔFOSB/JUND insensitive to redox changes but do not affect its DNA-binding properties, and larger compounds that exhibit both effects.

Our compounds elicit activating effects on the expression of an AP1 luciferase reporter gene in cell-based assays, regardless of whether they prevent ΔFOSB from binding to DNA in biochemical assays (e.g. Z2159931480) or not (e.g. 2196-99-8). When compounds covalently bind to the redox-switch cysteines, they necessarily protect the cysteines from disulfide-bond formation, but they may do so even if binding is not covalent. Although the smaller, fragment-like analogs such as 2196-99-8 might not be sufficient to disrupt DNA-binding in biochemical assays (similar to ΔFOSB Cys^{172}Trp), in cells, they may well prevent the oxidation of the redox switch and thus prevent the loss of DNA-binding capabilities, thus leading to a net activating effect on the ability of ΔFOSB to promote gene transcription, especially under oxidizing conditions. Additionally, our compounds could impact the biological function of ΔFOSB in the cellular context not just by working on the DNA-binding properties of ΔFOSB directly but also by altering its ability to bind to epigenetic factors or to integrate into the large transcriptional protein assemblies required for its function. Regarding our cell-based assays using AP1-luc HEK293 cells (Figure 6G and H), it is important to note that FBS stimulation generates a portfolio of distinct AP1 transcription factors, each with different trans-activational properties and protein half-lives. Thus, even though ΔFOSB dominates at the time point used, the observed activities of our compounds likely represent the aggregate effect on all AP1 transcription factors present following FBS stimulation, including those transcription factors that are not directly impacted by the compound at all. As an illustration, different ΔFOSB-containing species have different effects on transcription; expressing ΔFOSB, JUND, or both, directly in cells reveals that ΔFOSB/JUND heterodimers activate luciferase expression six to seven times more robustly than the respective homomers (Figure 7C). In addition, releasing ΔFOSB from the reporter gene through the action of the compounds may enable other transcription factors to dominate the overall transcription of that reporter. Our cellular assays, therefore, likely reveal the effect of our compounds on the portfolio of different transcription factor species through their respective protein levels and occupancies on the reporter gene, all of which coalesce into a 'net' activating transcriptional effect. Testing our compounds in cell lines with specific AP1 transcription factors knocked out will deconvolute the impact of our compounds on biological activity and assess their selectivity.

To gain insights into the capability of redox switch-seeking compounds to target different ΔFOSB-containing transcription factors selectively as well as all AP1 transcription factors as a whole, we examined the sequence conservation of human bZIP proteins around the compound-binding site (Figure 7D, E, and Supplementary Figure S6). There are 29 human bZIP proteins that carry a cysteine residue at a position equivalent to ΔFOSB Cys^{172} and JUND Cys^{285} (i.e. with consensus sequence Cys-$(X)_{10}$-Leu). We found that residues in the deep crevasse at the fulcrum of the bZIP forceps that bind to Z2159931480 and flank the DNA-binding motifs are highly conserved (Figure 7d). By contrast, residues lining the entrance of the crevasse are not conserved (e.g. JUND Lys^{274}, Ala^{281} and ΔFOSB Arg^{158}, Arg^{161}, Arg^{162}). These differences provide possible avenues to design compounds with unique selectivity for different AP1 transcription factors (Figure 7d). Furthermore, comparing ΔFOSB heterodimers and homomers by mapping the sequence conservation of FOS and JUN family members onto the crystal structure of ΔFOSB/$JUND^{red}$ bZIP (heterodimer) and ΔFOSB/ΔFOSB (homomer; PDB ID: 6UCL), respectively, reveals that though these sequences are highly conserved, the shapes of the binding pockets are dramatically different. This is because the ΔFOSB/JUND heterodimer adopts the canonical leucine zipper whereas ΔFOSB homomers adopt a non-canonical zipper that differs in how the helices are aligned with respect to each other (24,25) (structures in this study) (Figure 7E). The redox-switch cysteines thus provide covalent anchors at the base of a crevasse situated at the fulcrum of the bZIP forceps, which can now be further leveraged to design new modulators with selective properties.

DISCUSSION

The transcription factor ΔFOSB drives programs of gene expression that mediate stable neural and behavioral adaptations in response to many types of chronic stimuli involved in neurological and neuropsychiatric disorders, so it appears to be an attractive drug target (18). However, transcription factors are typically considered 'undruggable' (47) because they are thought to be devoid of pockets that support specific small-molecule binding. Also, bZIP tran-

scription factors like ΔFOSB are particularly challenging because the helices containing the DNA-binding motifs historically are thought to be disordered in solution in the absence of DNA (48,49). Recently, we revealed a putative redox switch formed by ΔFOSB Cys^{172} and JUND Cys^{285} that can regulate DNA-binding *in vitro* (24) and that is currently under investigation *in vivo* (18). Indeed, we have already demonstrated that in neuron-like cultured Neuro2a cells, ΔFOSB forms homomeric and heteromeric (e.g. with JunD) complexes that are stabilized by SDS-resistant covalent bonds that can be eliminated by reducing agents (25), suggesting that the putative redox switch can be engaged in cells under basal conditions. Cysteine-targeting compounds are an attractive strategy to vanquish 'undruggable' protein targets, an avenue that could be particularly useful for ΔFOSB because of its strategically located cysteine redox switch. Here, we: (a) identified compounds that target the redox switch of ΔFOSB; (b) validated their action in orthogonal biochemical assays and by mass spectrometry; (c) determined the crystal structures of the ΔFOSB/JUND bZIP in the absence and presence of one compound to reveal its binding mode, mechanism of action and 'theater of operations' for future structure-based compound optimization using medicinal chemistry; (d) demonstrated that redox switch-targeting compounds elicit biological effects on gene expression in cell-based assays and (e) show that these compounds are relatively non-toxic despite their potential to covalently bind proteins. Together, these data establish that the redox switch of ΔFOSB provides a path towards rendering this protein vulnerable to small molecules and that other members of the FOS/JUN family of transcription factors can likely be targeted using this strategy as well.

The ΔFOSB redox switch—an attractive molecular handle to regulate function

The redox switch in ΔFOSB/JUND is an attractive protein feature to 'drug'. It not only impacts DNA-binding properties directly but it can likely be leveraged to target ΔFOSB function more broadly, for instance, by inactivating specific pathogenic forms of ΔFOSB that accumulate *in vivo* (e.g. ΔFOSB homomers). Covalently modifying the cysteine residues of the ΔFOSB redox switch overcomes critical barriers that hamper traditional drug discovery strategies such as those used to target largely buried catalytic active sites. For example, it allows the accumulated protein to be long-lastingly targeted, even if a ΔFOSB molecule exchanges its partner (e.g. JUND, c-JUN or another copy of ΔFOSB) as a consequence of protein levels fluctuating within the cell. It can also overcome the flexible nature of the DNA-binding motifs and the large entropic penalties that in all probability accompany compound binding. Though the DNA-binding motifs (residues Asn^{165}-Arg^{173} in ΔFOSB and Asn^{278}-Arg^{286} in JUND) have been suggested to be disordered (48,49), they adopt folded α-helices in all crystal structures observed to date (24,25); Figures 2 and 5). Furthermore, representative Group A and Group B compounds are active against ΔFOSB even when the redox-switch residue Cys^{172} is mutated to serine (Figure 7a and Supplementary Figure S4). Thus, the compounds likely encounter a preformed binding pocket deep at the fulcrum of the bZIP forceps (or can efficiently induce one) and the DNA-binding motifs are folded at least partially or part of the time. Therefore, the redox switch offers a handle for attaching a portfolio of different moieties of various sizes and/or chemical properties, which could be further leveraged to fine-tune the function of ΔFOSB in different ways, e.g. by selectively blocking the response to oxidative stress while preserving, increasing, or decreasing its DNA-binding properties.

Druggability of the ΔFOSB redox switch

Our small molecule screen reveals that ΔFOSB Cys^{172} and JUND Cys^{285} are susceptible to compound binding in unique ways. Out of the 3200 compounds screened, we identified only three validated hits (Z2159931480, Z3247353427, Z2492395544) (<0.1% of the library) that disrupt DNA-binding, despite the library containing a large variety of different cysteine-targeting groups. Cysteines in proteins are chemically generally relatively inert, but their reactivity can vary considerably depending on their structural context. Deprotonation to thiolate yields a more reactive and nucleophilic species compared to the protonated state, with pK_a values falling in the range of 2.5–11.1 (29). Not all cysteine residues are susceptible to covalent modification, even when solvent-exposed (29), emphasizing their unique and individual properties. Hence, ΔFOSB Cys^{172} and JUND Cys^{285} likely have distinctive chemical reactivities. Steric considerations may also account for the low number of hits found for ΔFOSB; firstly, by determining whether a compound can fit at the base of the bZIP fulcrum, and secondly, by determining whether it can disrupt the interaction with DNA (our screening criterion). For example, the analogs in Group A are fragments of the original hit and contain the same reactive group. Nevertheless, while they bind to the redox-switch cysteines by MS, they do not disrupt DNA-binding in biochemical assays likely because they are too small. Hence, such compounds would not be identified in our initial screen. The existence of a preformed or inducible binding site at the fulcrum of the bZIP forceps is mechanistically important because it suggests that protein:ligand interactions might position reactive compounds with appropriate shape and chemical reactivity within strategic distance to the cysteine S^{γ}-atoms, permitting them to then bind covalently over time. Classes of compounds currently being used to target cysteines for drug discovery purposes often bind in such a two-step process: a compound carrying a weakly electrophilic warhead first reversibly associates, followed by the warhead covalently attaching to the appropriately positioned nucleophilic cysteine (50). Such a two-step, potentially slow, reversible, and mixed binding mode is more difficult to characterize (e.g. it confounds determining standard thermodynamic parameters, such as IC_{50} values). But it also provides opportunities to target the ΔFOSB redox switch in differentiating ways by exploiting the exact shape of the preformed pocket housing the redox-switch cysteines, any inherent structural plasticity, and the unique reactivities of the redox-switch cysteines.

In summary, our studies reveal that the redox switch of ΔFOSB is a promising platform for the development of selective compounds for modulating various aspects of

the ΔFOSB activity profile (Figure 7F). First, it is located at the base of a (preformed) binding site composed of folded DNA-binding regions, where it provides covalent anchors of limited reactivity. The binding pocket and redox switch can thus likely be exploited to stably alter ΔFOSB pathological species that accumulate, even upon their dissociation and reassembly with other bZIP partners, once a compound is stably covalently attached. Second, because the redox switch is part of the DNA-binding motifs, bound compounds are strategically positioned to affect a key biological function of ΔFOSB. Third, the switch is located at the interface between two bZIP partners, with one dimer partner supplying the reactive redox-switch cysteine to which a compound binds, while the other partner provides key residues that line the binding pocket. Accordingly, the compound-binding pocket is hybrid, and compounds could conceivably be designed to specifically recognize dimers of distinct FOS/JUN members. Fourth, the deep crevasse that houses the redox switch is suitably sized to accommodate drug-like compounds that can trigger different functional effects. Small compounds could block the redox switch protecting ΔFOSB from oxidative stress while leaving DNA-binding intact. Larger compounds could interact with unique 'selectivity' residues lining the pocket and/or exploit differences in the pocket shape between various ΔFOSB:partner combinations. Fifth, the binding pocket housing the redox switch is expandable in size due to the flexibility of the DNA-binding motifs. Combined, these features suggest that the redox switch constitutes a promising platform for the design of pharmacological agents that target ΔFOSB function in a directed fashion and that these can be engineered to be specific for a given bZIP partner.

Compound classes that target the ΔFOSB redox switch

Though more than 10 different classes of reactive groups were represented in the Enamine library screen, only two classes were identified as hits, the α-haloketones (Group A) and the acrylamides (Group B). Currently, acrylamides, α-halo carbonyl electrophiles, and α,β-unsaturated carbonyl compounds are the most often used reactive groups to target non-catalytic cysteine residues for drug discovery (29). Acrylamides, α-substituted acetylenes, and α-substituted halo-acetamides typically exhibit highly attenuated thiol reactivity making them suitable for developing compounds that are more target-selective (29,51). The Group B compound, Z3247353427, contains an acrylamide warhead that is very similar to that used in the FDA-approved drugs ibrutinib and zanubrutinib (50) (Figure 3c). The library that we screened (3200 compounds in total) contains 622 other compounds with an α-haloketone reactive group (Group A) and 1920 other compounds with an acrylamide reactive group (Group B), including compounds that carry both functional groups, yet strikingly, these were not identified as hits during our screening campaign indicating chemical selectivity (or the ability to escape our hit-identification criterion, i.e. disruption of DNA-binding).

Interesting differences are observed between Group A and Group B compounds, despite targeting the same protein feature in the ΔFOSB/JUND bZIP. Group A compounds robustly bind to the ΔFOSB/JUND bZIP by MS, while Group B compounds do not. It is possible that Group A compounds are chemically more reactive or yield more stable protein:compound complexes compared to Group B compounds. In cell-based assays, Group A compounds are much more potent activators of the luciferase reporter gene compared to Group B compounds. To explain these differences, both ΔFosB-dependent mechanisms (for example those pertaining to the stability of the protein:compound complex), as well as ΔFosB-independent mechanisms (for example those pertaining to the stability of just the compound), are conceivable. The increase in luciferase activity is not due to off-target effects, e.g. the compounds increasing luciferase activity (52) because they require FBS-stimulation of the AP1-luc HEK293 cells to robustly drive expression of the AP1-luciferase gene (i.e. the production of AP1 transcription factors including ΔFOSB). Interestingly, while Group A and Group B compounds disrupt the binding of recombinant, purified ΔFOSB/JUND heterodimers and ΔFOSB homomers to DNA to varying extents, they all increase the expression of the AP1-luciferase reporter. By contrast, T5224, which also disrupts DNA-binding, inhibits the expression of the AP1-luciferase reporter (Figure 6E and Supplementary Figure S4a). Also, our compounds show much greater potency in cell-based assays compared with biochemical assays using recombinant proteins, a phenomenon also observed for T5224 (Figure 3) (45). Do compounds that shield the redox switch from oxidation in cells induce unique conformations in the ΔFOSB protein that alter the way ΔFOSB integrates with other components of the transcriptional machinery? Or do they impact protein stability or subcellular localization? Are these compounds better described as modulators of ΔFosB function? Additional mechanistic studies will be needed to delineate compound action *ex vivo* and *in vivo*.

Future studies

There is a desperate need to identify drug targets for common, chronic conditions like drug addiction, depression, Alzheimer's disease, and Parkinson's disease-associated dyskinesias, all of which involve increased ΔFOSB protein levels in specific brain regions and cell types that are linked to their pathologies. It is estimated that only ∼2% of human proteins are currently targeted by small molecule drugs, while only 10–15% are thought to be druggable using traditional methods (53). The covalent modification of cysteines is developing into an effective avenue to target proteins previously considered to be 'undruggable' (29,50). Since 1990, the FDA has approved at least 32 drugs in the US that form covalent bonds with their target protein (50). Some cysteine-modifying drugs, such as the irreversible proton pump inhibitors omeprazole, esomeprazole, and lansoprazole for treating acid-reflux and peptic ulcers, feature a safety profile that allows them to be marketed over-the-counter (50). Key factors regulating the ability of a compound to covalently attach to a specific cysteine are rooted in: (i) the reactivity of the thiol group (which is influenced by neighboring residues); (ii) the nature of the compound-binding pocket or surface and (iii) the chemical properties of the electrophile that reacts with the thiolate and which can be altered through electron-withdrawing or

-donating groups at strategic positions in the compound (29,50,51,54,55). Not all cysteine residues present in the proteome are reactive; only ∼700 cysteine residues were found to be modified in human cancer cell lines when using a panel of chloroacetamide and acrylamide electrophiles (56). Interestingly, FOS and JUN proteins were not identified in this study, perhaps because AP1 transcription factors typically have very short half-lives. Because ΔFOSB has a very slow turnover rate in brain (9,20) and possesses a selectively accessible and reactive cysteine residue near the DNA-binding site (this paper), it is an attractive candidate to target with covalent cysteine-binding compounds. Such compounds could permit enduring therapies at low drug doses, thus minimizing the occurrence and severity of adverse reactions. The compounds identified in this work, therefore, serve as promising starting points to apply a 'scaffold morphing approach' (57) to optimize potency, pharmacokinetics/pharmacodynamics (PK/PD) properties, selectivity, as well as absorption, distribution, metabolism, and excretion (ADME) profiles.

DATA AVAILABILITY

Coordinates and structure factors for the crystal structures of ΔFOSB/JUND bZIP^{red} and ΔFOSB/JUND bZIP^{cmpd} have been deposited to PDB under the accession numbers 7UCC and 7UCD, respectively. The mass spectrometry proteomics data have been deposited to the ProteomeXchange Consortium via the PRIDE (58) partner repository with the dataset identifier PXD035839.

SUPPLEMENTARY DATA

Supplementary Data are available at NAR Online.

ACKNOWLEDGEMENTS

The Advanced Photon Source (sectors IMCA-CAT, LS-CAT, and SBC-CAT) and the Advanced Light Source are thanked for access to synchrotron radiation. We thank Mukund Bhandari, Ryan Murphy and Harikanth Venkannagari for preliminary pilot studies, and Haiying Chen for experimental assistance.

FUNDING

NIH/NIDA [R01DA040621 to A.J.R., E.J.N., G.R., J.Z., P01DA047233 to E.J.N.]; Sealy Center for Structural Biology and Molecular Biophysics (SCSB) at UTMB (to G.R.); Cancer Prevention Research Institute of Texas (CPRIT) [RP190682 to W.R.]; Cancer Prevention Research Institute of Texas (CPRIT) [RP150578 to C.S.]; Stuart & Suzanne Steele MGH Research Scholars Program (to S.J.H]); Jeane B. Kempner Fellowship Program and the UTMB Center for Addiction Research Predoctoral Fellowship [NIDA T32 DA 07287 to H.L.]; John D. Stobo, M.D. Distinguished Chair Endowment Fund (to J.Z.); Funding for open access charge: NIH/NIDA [R01DA040621].
Conflict of interest statement. None declared.

REFERENCES

1. Robison,A.J. and Nestler,E.J. (2011) Transcriptional and epigenetic mechanisms of addiction. *Nat. Rev. Neurosci.*, **12**, 623–637.
2. Nestler,E.J. (2015) ΔFosB: a transcriptional regulator of stress and antidepressant responses. *Eur. J. Pharmacol.*, **753**, 66–72.
3. Teague,C.D. and Nestler,E.J. (2022) Key transcription factors mediating cocaine-induced plasticity in the nucleus accumbens. *Mol. Psychiatry*, **27**, 687–709.
4. Nishijima,T., Kawakami,M. and Kita,I. (2013) Long-term exercise is a potent trigger for DeltaFosB induction in the hippocampus along the dorso-ventral axis. *PLoS One*, **8**, e81245.
5. Perrotti,L.I., Hadeishi,Y., Ulery,P.G., Barrot,M., Monteggia,L., Duman,R.S. and Nestler,E.J. (2004) Induction of deltaFosB in reward-related brain structures after chronic stress. *J. Neurosci.*, **24**, 10594–10602.
6. Hiroi,N., Marek,G.J., Brown,J.R., Ye,H., Saudou,F., Vaidya,V.A., Duman,R.S., Greenberg,M.E. and Nestler,E.J. (1998) Essential role of the fosB gene in molecular, cellular, and behavioral actions of chronic electroconvulsive seizures. *J. Neurosci.*, **18**, 6952–6962.
7. You,J.C., Muralidharan,K., Park,J.W., Petrof,I., Pyfer,M.S., Corbett,B.F., LaFrancois,J.J., Zheng,Y., Zhang,X., Mohila,C.A. *et al.* (2017) Epigenetic suppression of hippocampal calbindin-D28k by ΔFosB drives seizure-related cognitive deficits. *Nat. Med.*, **23**, 1377–1383.
8. Corbett,B.F., You,J.C., Zhang,X., Pyfer,M.S., Tosi,U., Iascone,D.M., Petrof,I., Hazra,A., Fu,C.-H., Stephens,G.S. *et al.* (2017) ΔFosB regulates gene expression and cognitive dysfunction in a mouse model of alzheimer's disease. *Cell Rep.*, **20**, 344–355.
9. Manning,C.E., Williams,E.S. and Robison,A.J. (2017) Reward network immediate early gene expression in mood disorders. *Front. Behav. Neurosci*, **11**, 77.
10. Vialou,V., Robison,A.J., Laplant,Q.C., Covington,H.E., Dietz,D.M., Ohnishi,Y.N., Mouzon,E., Rush,A.J., Watts,E.L., Wallace,D.L. *et al.* (2010) DeltaFosB in brain reward circuits mediates resilience to stress and antidepressant responses. *Nat. Neurosci.*, **13**, 745–752.
11. Aleyasin,H., Flanigan,M.E., Golden,S.A., Takahashi,A., Menard,C., Pfau,M.L., Multer,J., Pina,J., McCabe,K.A., Bhatti,N. *et al.* (2018) Cell-Type-Specific role of DeltaFosB in nucleus accumbens in modulating intermale aggression. *J. Neurosci.*, **38**, 5913–5924.
12. Quansah Amissah,R., Chometton,S., Calvez,J., Guevremont,G., Timofeeva,E. and Timofeev,I. (2020) Differential expression of DeltaFosB in reward processing regions between binge eating prone and resistant female rats. *Front. Syst. Neurosci.*, **14**, 562154.
13. Beck,G., Singh,A., Zhang,J., Potts,L.F., Woo,J.-M., Park,E.S., Mochizuki,H., Mouradian,M.M. and Papa,S.M. (2019) Role of striatal ΔFosB in l-Dopa-induced dyskinesias of parkinsonian nonhuman primates. *Proc. Natl. Acad. Sci. U.S.A.*, **116**, 18664–18672.
14. Eagle,A.L., Gajewski,P.A., Yang,M., Kechner,M.E., Al Masraf,B.S., Kennedy,P.J., Wang,H., Mazei-Robison,M.S. and Robison,A.J. (2015) Experience-Dependent induction of hippocampal ΔFosB controls learning. *J. Neurosci.*, **35**, 13773–13783.
15. Lafragette,A., Bardo,M.T., Lardeux,V., Solinas,M. and Thiriet,N. (2017) Reduction of cocaine-induced locomotor effects by enriched environment is associated with cell-specific accumulation of DeltaFosB in striatal and cortical subregions. *Int. J. Neuropsychopharmacol.*, **20**, 237–246.
16. Pollema-Mays,S.L., Centeno,M.V., Chang,Z., Apkarian,A.V. and Martina,M. (2019) Reduced DeltaFosB expression in the rat nucleus accumbens has causal role in the neuropathic pain phenotype. *Neurosci. Lett.*, **702**, 77–83.
17. Nestler,E.J., Kelz,M.B. and Chen,J. (1999) DeltaFosB: a molecular mediator of long-term neural and behavioral plasticity. *Brain Res.*, **835**, 10–17.
18. Robison,A.J. and Nestler,E.J. (2022) DeltaFOSB: a potentially druggable master orchestrator of activity-dependent gene expression. *ACS Chem. Neurosci.*, **13**, 296–307.
19. Beck,G., Zhang,J., Fong,K., Mochizuki,H., Mouradian,M.M. and Papa,S.M. (2021) Striatal DeltaFosB gene suppression inhibits the development of abnormal involuntary movements induced by L-Dopa in rats. *Gene Ther.*, **28**, 760–770.
20. Ulery-Reynolds,P.G., Castillo,M.A., Vialou,V., Russo,S.J. and Nestler,E.J. (2009) Phosphorylation of DeltaFosB mediates its stability in vivo. *Neuroscience*, **158**, 369–372.

21. Carle,T.L., Ohnishi,Y.N., Ohnishi,Y.H., Alibhai,I.N., Wilkinson,M.B., Kumar,A. and Nestler,E.J. (2007) Proteasome-dependent and -independent mechanisms for FosB destabilization: identification of FosB degron domains and implications for DeltaFosB stability. *Eur. J. Neurosci.*, **25**, 3009–3019.
22. Robison,A.J., Vialou,V., Mazei-Robison,M., Feng,J., Kourrich,S., Collins,M., Wee,S., Koob,G., Turecki,G., Neve,R. *et al.* (2013) Behavioral and structural responses to chronic cocaine require a feedforward loop involving ΔFosB and calcium/calmodulin-dependent protein kinase II in the nucleus accumbens shell. *J. Neurosci.*, **33**, 4295–4307.
23. Jorissen,H.J.M.M., Ulery,P.G., Henry,L., Gourneni,S., Nestler,E.J. and Rudenko,G. (2007) Dimerization and DNA-binding properties of the transcription factor deltafosB. *Biochemistry*, **46**, 8360–8372.
24. Yin,Z., Machius,M., Nestler,E.J. and Rudenko,G. (2017) Activator protein-1: redox switch controlling structure and DNA-binding. *Nucleic. Acids. Res.*, **45**, 11425–11436.
25. Yin,Z., Venkannagari,H., Lynch,H., Aglyamova,G., Bhandari,M., Machius,M., Nestler,E.J., Robison,A.J. and Rudenko,G. (2020) Self-assembly of the bZIP transcription factor ΔFosB. *Curr. Res. Struct. Biol.*, **2**, 1–13.
26. Chen,J., Nye,H.E., Kelz,M.B., Hiroi,N., Nakabeppu,Y., Hope,B.T. and Nestler,E.J. (1995) Regulation of delta FosB and fosb-like proteins by electroconvulsive seizure and cocaine treatments. *Mol. Pharmacol.*, **48**, 880–889.
27. Abate,C., Patel,L., Rauscher,F.J. and Curran,T. (1990) Redox regulation of fos and jun DNA-binding activity in vitro. *Science*, **249**, 1157–1161.
28. Bauer,R.A. (2015) Covalent inhibitors in drug discovery: from accidental discoveries to avoided liabilities and designed therapies. *Drug Discov. Today*, **20**, 1061–1073.
29. Gehringer,M. and Laufer,S.A. (2019) Emerging and re-emerging warheads for targeted covalent inhibitors: applications in medicinal chemistry and chemical biology. *J. Med. Chem.*, **62**, 5673–5724.
30. Wang,Y., Cesena,T.I., Ohnishi,Y., Burger-Caplan,R., Lam,V., Kirchhoff,P.D., Larsen,S.D., Larsen,M.J., Nestler,E.J. and Rudenko,G. (2012) Small molecule screening identifies regulators of the transcription factor ΔFosB. *ACS Chem. Neurosci.*, **3**, 546–556.
31. Markossian,S., Grossman,A., Brimacombe,K., Arkin,M., Auld,D., Austin,C.P., Baell,J., Chung,T.D.Y., Coussens,N.P. and Dahlin,J.L. *et al.*2004) In: *Assay Guidance Manual*. Bethesda (MD).
32. Li,Y., Liu,Z., Aglyamova,G., Chen,J., Chen,H., Bhandari,M., White,M.A., Rudenko,G. and Zhou,J. (2020) Discovery of phenanthridine analogues as novel chemical probes disrupting the binding of DNA to ΔFosB homodimers and ΔFosB/JunD heterodimers. *Bioorg. Med. Chem. Lett.*, **30**, 127300.
33. Shah,B., Jiang,X.G., Chen,L. and Zhang,Z. (2014) LC-MS/MS peptide mapping with automated data processing for routine profiling of N-glycans in immunoglobulins. *J. Am. Soc. Mass. Spectrom.*, **25**, 999–1011.
34. Zhang,Z., Pan,H. and Chen,X. (2009) Mass spectrometry for structural characterization of therapeutic antibodies. *Mass Spectrom. Rev.*, **28**, 147–176.
35. Otwinowski,Z. and Minor,W. (1997) Processing of X-ray diffraction data collected in oscillation mode. *Macromol. Crystallogr. A*, **276**, 307–326.
36. Kabsch,W. (2010) Xds. *Acta Crystallogr. Biol. Crystallogr.*, **66**, 125–132.
37. Kabsch,W. (2010) Integration, scaling, space-group assignment and post-refinement. *Acta Crystallogr. Biol. Crystallogr.*, **66**, 133–144.
38. McCoy,A.J., Grosse-Kunstleve,R.W., Adams,P.D., Winn,M.D., Storoni,L.C. and Read,R.J. (2007) Phaser crystallographic software. *J. Appl. Crystallogr.*, **40**, 658–674.
39. Adams,P.D., Afonine,P.V., Bunkóczi,G., Chen,V.B., Davis,I.W., Echols,N., Headd,J.J., Hung,L.-W., Kapral,G.J., Grosse-Kunstleve,R.W. *et al.* (2010) PHENIX: a comprehensive Python-based system for macromolecular structure solution. *Acta Crystallogr. D Biol. Crystallogr.*, **66**, 213–221.
40. Emsley,P., Lohkamp,B., Scott,W.G. and Cowtan,K. (2010) Features and development of coot. *Acta Crystallogr. D Biol. Crystallogr.*, **66**, 486–501.
41. Williams,C.J., Headd,J.J., Moriarty,N.W., Prisant,M.G., Videau,L.L., Deis,L.N., Verma,V., Keedy,D.A., Hintze,B.J., Chen,V.B. *et al.* (2018) MolProbity: more and better reference data for improved all-atom structure validation. *Protein Sci. Publ. Protein Soc.*, **27**, 293–315.
42. Sheridan,S.D., Theriault,K.M., Reis,S.A., Zhou,F., Madison,J.M., Daheron,L., Loring,J.F. and Haggarty,S.J. (2011) Epigenetic characterization of the FMR1 gene and aberrant neurodevelopment in human induced pluripotent stem cell models of fragile x syndrome. *PLoS One*, **6**, e26203.
43. Cates,H.M., Thibault,M., Pfau,M., Heller,E., Eagle,A., Gajewski,P., Bagot,R., Colangelo,C., Abbott,T., Rudenko,G. *et al.* (2014) Threonine 149 phosphorylation enhances ΔFosB transcriptional activity to control psychomotor responses to cocaine. *J. Neurosci.*, **34**, 11461–11469.
44. Bossis,G., Malnou,C.E., Farras,R., Andermarcher,E., Hipskind,R., Rodriguez,M., Schmidt,D., Muller,S., Jariel-Encontre,I. and Piechaczyk,M. (2005) Down-regulation of c-Fos/c-Jun AP-1 dimer activity by sumoylation. *Mol. Cell. Biol.*, **25**, 6964–6979.
45. Aikawa,Y., Morimoto,K., Yamamoto,T., Chaki,H., Hashiramoto,A., Narita,H., Hirono,S. and Shiozawa,S. (2008) Treatment of arthritis with a selective inhibitor of c-Fos/activator protein-1. *Nat. Biotechnol.*, **26**, 817–823.
46. Ye,N., Ding,Y., Wild,C., Shen,Q. and Zhou,J. (2014) Small molecule inhibitors targeting activator protein 1 (AP-1). *J. Med. Chem.*, **57**, 6930–6948.
47. Henley,M.J. and Koehler,A.N. (2021) Advances in targeting 'undruggable' transcription factors with small molecules. *Nat. Rev. Drug Discov.*, **20**, 669–688.
48. Miller,M. (2009) The importance of being flexible: the case of basic region leucine zipper transcriptional regulators. *Curr. Protein Pept. Sci.*, **10**, 244–269.
49. Das,R.K., Crick,S.L. and Pappu,R.V. (2012) N-terminal segments modulate the α-helical propensities of the intrinsically disordered basic regions of bZIP proteins. *J. Mol. Biol.*, **416**, 287–299.
50. Roskoski,R., Jr. (2021) Orally effective FDA-approved protein kinase targeted covalent inhibitors (TCIs). *Pharmacol. Res.*, **165**, 105422.
51. Backus,K.M., Cao,J. and Maddox,S.M. (2019) Opportunities and challenges for the development of covalent chemical immunomodulators. *Bioorg. Med. Chem.*, **27**, 3421–3439.
52. Auld,D.S., Thorne,N., Nguyen,D.T. and Inglese,J. (2008) A specific mechanism for nonspecific activation in reporter-gene assays. *ACS Chem. Biol.*, **3**, 463–470.
53. Roberts,A.M., Ward,C.C. and Nomura,D.K. (2017) Activity-based protein profiling for mapping and pharmacologically interrogating proteome-wide ligandable hotspots. *Curr. Opin. Biotechnol.*, **43**, 25–33.
54. Baillie,T.A. (2016) Targeted covalent inhibitors for drug design. *Angew. Chem. Int. Ed Engl.*, **55**, 13408–13421.
55. Maurais,A.J. and Weerapana,E. (2019) Reactive-cysteine profiling for drug discovery. *Curr. Opin. Chem. Biol.*, **50**, 29–36.
56. Backus,K.M., Correia,B.E., Lum,K.M., Forli,S., Horning,B.D., González-Páez,G.E., Chatterjee,S., Lanning,B.R., Teijaro,J.R., Olson,A.J. *et al.* (2016) Proteome-wide covalent ligand discovery in native biological systems. *Nature*, **534**, 570–574.
57. Sun,H., Tawa,G. and Wallqvist,A. (2012) Classification of scaffold-hopping approaches. *Drug Discov. Today*, **17**, 310–324.
58. Perez-Riverol,Y., Bai,J., Bandla,C., Hewapathirana,S., García-Seisdedos,D., Kamatchinathan,S., Kundu,D., Prakash,A., Frericks-Zipper,A., Eisenacher,M. *et al.* (2022) The PRIDE database resources in 2022: a hub for mass spectrometry-based proteomics evidences. *Nucleic Acids Res.*, **50**, D543–D552.